Hadley Circulations in Radiative–Convective Equilibrium in an Axially Symmetric Atmosphere

MASAKI SATOH

Center for Climate System Research, University of Tokyo, Tokyo, Meguro, Japan

(Manuscript received 19 April 1993, in final form 14 December 1993)

ABSTRACT

Hadley circulations in radiative–convective equilibrium are investigated using an idealistic axially symmetric model. Calculations show that the distribution of temperature in the Hadley cell is controlled by the moist process; the vertical profiles are close to the moist-adiabatic profile in the precipitating ascent branch, and the latitudinal distribution is nearly uniform. A sharp meridional temperature gradient exists within the poleward sloping boundary of the cell. Similar to Held and Hou, the latitudinal gradient of the vertically averaged temperature is determined by the cyclostrophic wind balance with the angular momentum–conserving flow in the upper layer.

The region where the Hadley cell exists can easily be predicted from the relationship between the profiles of the surface temperature and the vertically averaged temperature. Under the condition that the solar flux is specified, however, because of the interaction between the atmospheric circulation and the surface temperature, the behavior of the Hadley cell is a little more complicated. In particular, if the rotation rate is faster than or equal to the terrestrial value, two peaks of the upward motion exist on both sides of the equator.

Contrary to the traditional view of a steady indirect cell (the Ferrel cell), a systematic multicell structure exists in the middle and high latitudes. The horizontal scale of the cells is about 1000 km. They move equatorward at a speed of ~ 1 m s^{-1}.

1. Introduction

The Hadley circulation is, in general, regarded as a horizontally convective cell driven by the north–south gradient of solar radiation heating. However, the differences of the solar heating in lower latitudes are not directly reflected to the atmospheric temperature, since most of the incident solar flux reaches the surface and the energy input into the atmosphere from the surface is in the form of latent heat. The latent heat supplied from the surface is transported equatorward by the low-level flow and is released as a cumulus heating in the intertropical convergence zone (ITCZ). The released heat is retransported poleward by the upper-level flow to the subtropical latitudes, where the air is cooled by radiation. In such a manner, in the region of the Hadley circulation, a balance exists among the supply of the latent heat from the surface, the heat transport by the circulation, and the radiative cooling in the free atmosphere (e.g., Lorenz 1967; Oort and Peixóto 1983). In this sense, the Hadley circulation can be thought of as a vertically convective cell in the radiative–convective equilibrium.

Radiative–convective equilibrium is mostly considered by using one-dimensional models. The convective part of it is naturally a horizontal average of every kind of circulations existing in the atmosphere: not only small-scale eddies in the tropics and the middle and high latitudes but also large-scale circulations such as the Hadley circulation and baroclinic waves (e.g., Manabe and Strickler 1964; Ramanathan and Coakley 1978). Among them, the Hadley circulation contributes to a major part of the vertical transport of energy in the tropics (Riehl and Malkus 1958), so that it must be taken into account as convections of the radiative–convective equilibrium (Satoh and Hayashi 1992, section 5).

The understanding of the dynamics of the Hadley circulation has been promoted by the studies of axially symmetric models by Schneider (1977) and Held and Hou (1980) (hereafter referred to as S77, HH80, respectively). The energy balance employed by HH80 was a simple form of a Newtonian cooling; the heating is given to be proportional to the difference between the calculated potential temperature and the externally specified state θ_e. Various properties of the Hadley circulation have been studied using Newtonian cooling after HH80. Lindzen and Hou (1988) examined the

Corresponding author address: Dr. Masaki Satoh, Department of Mechanical Engineering, Saitama Institute of Technology, 1690 Fusaiji, Okabe, Oosato, Saitama 369-02, Japan.

seasonal variation of the Hadley cell by adopting asymmetric heating profiles centered off the equator, and showed that the winter cell became much stronger than the summer cell even when the peak latitude of θ_e was shifted to 2°. As an extension of this study, Hou and Lindzen (1992) showed that the concentration of the heating increased the intensity of the circulation. Schneider (1983) applied the simple theory of HH80 to the Martian dust storms, and found that different local and global response regimes of a circulation to heating existed concentrated in a small-latitude band. Hou (1984) discussed the Venus circulation by extending the theory of HH80 to slowly rotating atmospheres. Plumb and Hou (1992) showed that, in response to localized heating forcing, there was a transition behavior from a steady state of thermal equilibrium with no meridional flow to a strong meridional circulation.

HH80 and subsequent studies assumed a statically stable state as a vertical profile of θ_e. In general, one-dimensional "radiative" equilibrium is statically unstable, so that the possibility of small-scale convections occurring exist at every latitude (Manabe and Möller 1961). If the small-scale convections take place with latent heat release, the temperature will follow a moist-adiabatic profile (Sarachik 1978; Satoh and Hayashi 1992), which is a stable stratification for the dry process. Hence, the stable θ_e should be regarded as a consequence of one-dimensional "radiative–convective" equilibrium with small-scale moist convections at each latitude. It also implies that the small-scale convections are independent of the meridional circulation (HH80, section 2; Schneider 1983, section 2).

It is not appropriate, however, to assume that the small-scale convections are independent of the meridional circulation, since subsidence motion of the Hadley circulation suppresses deep convection in the subtropics in the real atmosphere. HH80 argue that the process of the latent heat release can be incorporated by modifying the meridional distribution of θ_e (HH80, section 6). Hou and Lindzen (1992) followed this argument, and examined the effect of cumulus heating on the width and the strength of the Hadley circulations by altering the concentration of θ_e. However, it is difficult to obtain a consistent view between the Hadley circulation and the water cycle by this procedure. It does not give a sufficient answer as to how the Hadley circulation behaves in radiative–convective equilibrium.

Hunt (1973) and Williams (1988b) have calculated radiative–convective equilibrium of an axisymmetric atmosphere using a two-dimensional zonally symmetric version of the general circulation models (GCM). The cell structures of their results are more complicated than those of S77 and HH80. The moist calculation of Hunt (1973) has an intense indirect cell in the tropical troposphere. The circulations of Williams (1988b) consist of one or two jets and one or two pairs of cells, though they are qualitatively similar to HH80 in the sense that the width of the Hadley cell becomes smaller as the rotation rate increases. Williams argues that, because of the nonlinearity of the latent heat release, the axisymmetric states have more complex cell structures than the three-dimensional states. He says that the scale of the cells of the axisymmetric states remains unexplained (Williams 1988b, section 2.1).

In the present study, using an axisymmetric numerical model with simple but physically based schemes for the processes of radiation and moist convection, the behaviors of the Hadley circulation in radiative–convective equilibrium are investigated. Section 2 describes the axisymmetric model used in this study. In contrast to Newtonian cooling with a statically stable reference state, the radiative cooling in the troposphere tends to create statically unstable states. The model is utilized to study what kind of circulations is produced, when no a priori assumptions are imposed between vertical convection and meridional circulation. Calculations for two types of boundary conditions for the surface temperature will be shown: one is the case where the distribution of the surface temperature is externally fixed (section 3a) and the other is the case where the solar flux is fixed and the surface temperature is calculated from the balance requirement of the energy (section 3b). In section 4, a simple model is constructed for the interpretation of the numerical results and is compared with that of HH80. In section 5, the simple model is extended to more general distributions of the surface temperature.

2. The axisymmetric model

Since this research deals with an idealistic axisymmetric system, which does not exist in the real atmosphere in the strict sense, the model is formulated in such a way that it is easy to gain physical understanding of the circulation structure in the model. For this purpose, simple and clear schemes are used for the physical processes such as radiation, convection, and diffusion, instead of elaborate schemes employed in ordinary climate models.

a. Basic equations

The numerical model is based on the primitive equations for two-dimensional motions:

$$\frac{\partial p_s}{\partial t} = -\frac{1}{a\cos\varphi}\frac{\partial}{\partial\varphi}(\cos\varphi p_s v) - \frac{\partial}{\partial\sigma}(p_s\dot{\sigma}), \tag{1}$$

$$\frac{dl}{dt} = a\cos\varphi f_\lambda, \tag{2}$$

$$\frac{dv}{dt} = -\frac{\sin\varphi}{a^3\cos^3\varphi}l^2 - \frac{1}{a\rho}\frac{\partial p}{\partial\varphi} - \frac{1}{a}\frac{\partial}{\partial\varphi}(\Phi + \Phi_C) + f_\varphi, \tag{3}$$

$$0 = -\frac{p_s}{\rho} - \frac{\partial \Phi}{\partial \sigma}, \tag{4}$$

$$\frac{dh}{dt} = \frac{1}{\rho}\frac{dp}{dt} - \frac{1}{\rho}Q^{\text{rad}} + \frac{1}{\rho}Q^{\text{dif}} + \frac{1}{\rho}Q^{\text{fric}}, \tag{5}$$

$$\frac{dq}{dt} = \frac{1}{\rho}S^{\text{dif}} - \frac{1}{\rho}S^{\text{prc}}. \tag{6}$$

The vertical coordinate is σ, where $\sigma = p/p_s$, p the pressure, and p_s the surface pressure. Equation (1) is the equation of mass conservation, where v is the meridional wind, $\dot{\sigma} \equiv d\sigma/dt$, φ is the latitude, and a the planetary radius. Equation (2) is the equation of angular momentum conservation, where

$$l = ua\cos\varphi + \Omega a^2 \cos^2\varphi \tag{7}$$

is the angular momentum, Ω the rotation rate, and f_λ the frictional term. Equation (3) is the equation of meridional wind, where $\Phi = gz$ is the gravitational potential, $\Phi_C = -a^2\Omega^2 \cos^2\varphi/2$ the centrifugal potential, f_φ is the frictional term, and ρ the density. Equation (4) is the equation of the hydrostatic balance. Equation (5) is the equation of moist enthalpy, where

$$h = C_pT + Lq \tag{8}$$

is the enthalpy for which C_p is the specific heat at constant pressure, T the temperature, L the latent heat, and q the specific humidity; Q^{rad} is the cooling by the radiation, Q^{dif} is the convergence of the diffusion of enthalpy, and Q^{fric} is the heating due to the frictional dissipation. Equation (6) is the equation of the specific humidity, where S^{dif} is the convergence of the diffusion of water vapor and S^{prc} is the change due to the precipitation.

The numerical model is integrated for the variables p_s, l, v, h, and q. The region considered is $-90°$ to $+90°$ in latitude, and σ is 0 to 1. The latitudinal grid has 100 points at intervals of $\Delta \sin\varphi = 0.02$, and the vertical grid has 50 points at intervals of $\Delta\sigma = 0.02$. Finite differentiation for the vertical coordinate is based on Arakawa and Suarez (1983), and the angular momentum and centrifugal force are discretized so as to conserve the total kinetic energy.

b. Radiative process

A simple nonscattering gray radiative model is used (Goody and Yung 1989; Satoh and Hayashi 1992). The solar radiation F_s is assumed to reach the surface without absorption in the atmosphere. The planetary radiative flux F_p is calculated from the equations of transfer using the temperature T and the optical thickness τ^* (Satoh and Hayashi 1992, appendix B). The distribution of τ^* is parameterized as a function of pressure by

$$\frac{\tau^*}{\tau_s^*} = \left(\frac{p}{p_s}\right)^\alpha, \tag{9}$$

where τ_s^* is the total optical thickness and α is a constant. The values $\tau_s^* = 2.0$, $\alpha = 2.0$ are used. The radiative cooling is expressed by

$$Q^{\text{rad}}(z) = \frac{d}{dz}[-F_s + F_p(z)]. \tag{10}$$

The solar flux F_s does not play any role in section 3a, where the surface temperature is externally fixed as a boundary condition.

c. Convective process

Consideration of vertical convections is required in order to stabilize the stratification of the model atmosphere. For this purpose, parameterized dry and moist convections are generally incorporated into numerical models. Hunt (1973) and Williams (1988b) used dry and moist adjustment schemes (Manabe et al. 1965) in their two-dimensional axisymmetric GCMs. Schneider and Lindzen (1977) and S77 parameterized moist convection by specifying vertical profiles of cumulus heating. In S77 and HH80, no consideration of the dry convection was required, because stable stratification was maintained by the Newtonian cooling.

In the present study, the following three schemes are employed because of their simplicity and clearness for physical interpretation. Dependencies on the schemes are summarized in the appendix.

The first scheme is one with no parameterization of convection, which is based on no a priori assumptions between large-scale motions and small-scale convections. Moist and dry convections are expected to be naturally resolved in the model. When water vapor content exceeds its saturated value, the excess is removed from the system as precipitation. This procedure corresponds to "large-scale condensation" usually employed in GCMs.

Both of the second and the third schemes are convective adjustment, but they are different in respect of vertical transportation of the angular momentum. In the convective adjustment scheme, the temperature is adjusted to the adiabatic profile, when the lapse rate is larger than the adiabatic value. This procedure is based on the assumption that the vertical mixing occurs rapidly and stabilizes stratification if a statically unstable state is produced within successive grid points in the vertical direction. As for the momentum transport, no particular consideration is generally made in cumulus models used in GCMs, even though cumulus friction is sometimes recalled (Schneider and Lindzen 1976). In a two-dimensional model, however, the angular momentum is a conserved quantity, so that it is physically natural to mix the angular momentum, in addition to the static energy and the specific humidity, in the col-

umn where adjustment occurs. In the present study, therefore, two kinds of schemes with and without vertical mixing of the angular momentum are compared. The meridional wind, in contrast, is not changed during adjustment for both schemes, since it is not a conserved quantity.

d. Diffusive process

The frictional terms f_λ and f_φ in Eqs. (2) and (3) are given, by analogy with molecular viscosity (e.g., Landau and Lifshits 1987), by

$$f_\lambda = \frac{1}{\rho}\left[\frac{1}{a\cos^2\varphi}\frac{\partial}{\partial\varphi}(\sigma'_{\lambda\varphi}\cos^2\varphi) + \frac{\partial}{\partial z}\sigma'_{\lambda z}\right], \quad (11)$$

$$f_\varphi = \frac{1}{\rho}\left[\frac{1}{a\cos\varphi}\frac{\partial}{\partial\varphi}(\sigma'_{\varphi\varphi}\cos\varphi) + \frac{\partial}{\partial z}\sigma'_{\varphi z}\right], \quad (12)$$

where $\sigma'_{ij}(i, j = \lambda, \varphi, z)$ are viscous stress tensors

$$\sigma'_{\lambda\varphi} = \rho\nu\frac{\cos\varphi}{a}\frac{\partial}{\partial\varphi}\left(\frac{u}{\cos\varphi}\right),$$

$$\sigma'_{\varphi\varphi} = 2\rho\nu\frac{1}{a}\frac{\partial v}{\partial\varphi}, \quad (13)$$

$$\sigma'_{\lambda z} = \rho\nu\frac{\partial u}{\partial z}, \quad \sigma'_{\varphi z} = \rho\nu\frac{\partial v}{\partial z}. \quad (14)$$

Here ν is the coefficient of viscosity. Corresponding to these expressions, the dissipation term Q^{fric} in the equation of enthalpy is expressed by

$$Q^{\text{fric}} = \rho\nu\left\{\left[\frac{\cos\varphi}{a}\frac{\partial}{\partial\varphi}\left(\frac{u}{\cos\varphi}\right)\right]^2 + \left(\frac{1}{a}\frac{\partial v}{\partial\varphi}\right)^2 + \left(\frac{\partial u}{\partial z}\right)^2 + \left(\frac{\partial v}{\partial z}\right)^2\right\}. \quad (15)$$

The diffusion terms Q^{dif} and S^{dif} in Eqs. (5) and (6) are given by

$$Q^{\text{dif}} = -\nabla\cdot(\mathbf{F}^{\text{dif}} + L\mathbf{i}), \quad (16)$$

$$S^{\text{dif}} = -\nabla\cdot\mathbf{i}. \quad (17)$$

Here $\mathbf{F}^{\text{dif}}$ and $\mathbf{i}$ are the diffusive fluxes of heat and specific humidity, given by

$$\mathbf{F}^{\text{dif}} = -\rho\kappa_h\nabla(C_pT + gz), \quad (18)$$

$$\mathbf{i} = -\rho\kappa_q\nabla q, \quad (19)$$

where κ_h, κ_q are the coefficients of diffusion for heat and specific humidity. The values of the coefficients are set to be uniform in the atmosphere. The parametric values used in the "standard case" are given in Table 1. No difference is imposed on the coefficients for meridional and vertical directions, so that meridional diffusions are almost negligible. Small values are given to κ_h and κ_q, since it is undesirable that the diffusions affect the stratification.

TABLE 1. Parameters.

Rotation rate	$\Omega_0 = 7.2722 \times 10^{-5}$ rad s^{-1}
Coefficient of viscosity	$\nu = \nu_s = 5$ m^2 s^{-1}
Coefficient of diffusion for heat	$\kappa_h = \kappa_{hs} = 1$ m^2 s^{-1}
Coefficient of diffusion for specific humidity	$\kappa_q = \kappa_{qs} = 1$ m^2 s^{-1}
Surface temperature (at the equator)	$T_s(0°) = 300$ K
Surface temperature (at the poles)	$T_s(\pm 90°) = 260$ K
Initial atmospheric temperature	$T(t = 0) = 250$ K
Total optical thickness	$\tau^* = 2.0$
Constant representing the profile of absorbing constituents	$\alpha = 2.0$
Mean surface pressure	$\bar{p}_s = 1013.25$ hPa
Planetary radius	$a = 6.37 \times 10^6$ m
Acceleration due to gravity	$g = 9.8$ m s^{-2}
Heat capacity for constant pressure	$C_p = 1.005 \times 10^3$ J kg^{-1} K^{-1}
Latent heat	$L = 2.5008 \times 10^6$ J kg^{-1}

e. Boundary conditions

As a boundary condition for the surface temperature, the following two cases will be investigated: the case where the surface temperature T_s is fixed and the case where the solar flux F_s is fixed and the surface temperature is calculated from the balance requirement of the energy at every time and every latitude (the "swamp" condition):

$$0 = S_h + LE + F_s - F_p(z = 0), \quad (20)$$

where S_h and E are the sensible heat flux and the evaporation of water vapor from the surface [see Eqs. (23) and (24)]. Experiments under these boundary conditions will be referred to as the fixed surface temperature condition and the fixed solar flux condition, respectively. At the surface, nonslip boundary conditions are imposed on the velocity fields, and the specific humidity is saturated. The diffusive fluxes at the top of the atmosphere are set to vanish.

The surface fluxes are rewritten in the "bulk formulas" from Eqs. (14), (18), and (19) as

$$\sigma'_{\lambda z}(z = 0) = \rho_s(C_DV)_m u_1, \quad (21)$$

$$\sigma'_{\varphi z}(z = 0) = \rho_s(C_DV)_m v_1, \quad (22)$$

$$S_h \equiv F_z^{\text{dif}}(z = 0) = \rho_s(C_DV)_h[C_p(T_s - T_1) + g\Delta z], \quad (23)$$

$$E \equiv i_z(z = 0) = \rho_s(C_DV)_q[q^*(p_s, T_s) - q_1], \quad (24)$$

where $(\ )_1$ denotes the value at the lowest level and $(\ )_s$ the value at the surface. Here $\Delta z = p_s \Delta\sigma / \rho_s g$ is the height at the lowest level, where $\Delta\sigma = \sigma_s - \sigma_1 = 0.01$; $q^*(p, T)$ denotes a saturated specific humidity at pressure p and temperature T. The bulk coefficients are expressed by

$$(C_D V)_m = \frac{\nu_s}{\Delta z}, \quad (C_D V)_h = \frac{\kappa_{hs}}{\Delta z},$$

$$(C_D V)_q = \frac{\kappa_{qs}}{\Delta z}, \tag{25}$$

where ν_s, κ_{hs}, and κ_{qs} are the coefficients of diffusion at the surface. The same values as the free atmosphere are given to the surface coefficients in the standard case.

f. Initial condition and time integration

The initial condition adopted in all calculations is a state at rest ($u = 0, v = 0$), a constant surface pressure ($p_s = 1013.25$ hPa), a constant atmospheric temperature ($T = 250$ K), and no humidity ($q = 0$). The time integration is performed using the Euler backward scheme (Matsuno scheme), with a time step of $\Delta t = 2$ or 3 minutes. The troposphere is statistically equilibrated in about 100 days under the fixed surface temperature condition, so that the equilibrium states are defined by averaging 100–150 days. Under the fixed solar flux condition, a global energy balance is satisfied in about 200 days, so that the equilibrium states are defined by averaging 250–300 days.

3. Results

a. The fixed surface temperature condition

Calculations are shown for the cases where the surface temperature is specified as

$$T_s(\varphi) = T_A - (T_B - T_A) \sin^2\varphi, \tag{26}$$

where $T_A = 300$ K, $T_B = 260$ K are given. As shown in the appendix, circulation structures are almost the same among three cases of different cumulus schemes. Therefore, only the results with no cumulus parameterization are shown in this subsection as the simplest case, and the results with cumulus adjustment are omitted.

Figure 1 shows the mass streamfunctions of the equilibrium states for various values of the rotation rate, $\Omega = 0$, 0.1, 1, and 10 ($\times\Omega_0$), where Ω_0 is the terrestrial value. In the standard case (Fig. 1c), a systematic meridional circulation exists in the latitudes from the equator to about 20° in the upper layers and to about 10° in the lower layers. This meridional circulation corresponds to the "Hadley circulation," though the width is somewhat smaller than that of the real atmosphere. In the poleward regions of the Hadley circulation exist localized vertical convections. It should be noted that a steady indirect cell (the Ferrel cell) does not exist in the middle and high latitudes. The "troposphere," which consists of the Hadley circulation and the localized vertical convections, extends from the surface to the "tropopause," and the "stratosphere" extends from the tropopause to the top of the model atmosphere. The height of the tropopause is about 300 hPa at the equator and becomes lower as latitude increases. Because of the simplified radiative scheme, the tropopause height is much lower than that of the real atmosphere. The width of the Hadley circulation becomes broader as Ω decreases; it is confined to about 2° for $\Omega = 10\Omega_0$ while it is global for $\Omega = 0$.

Figure 1 has an unrealistic character in that the streamfunction is not concentrated in the boundary layers near the surface and the tropopause. This is ascribed to the radiation property of the gray model. When averaged over the Hadley cell horizontally, the radiative cooling is balanced with the vertical energy convergence by the Hadley circulation. In this sense, the profile of the radiative cooling controls the distribution of the streamlines of the Hadley cell (Satoh and Hayashi 1992, section 5). On the other hand, the cooling profile does not depend on the circulation but on profiles of temperature and absorbing quantities (though the distribution of water vapor, which is the most active absorbing constituent, is affected by the circulation, in reality). The cooling profile for the gray model has a maximum in the middle troposphere, while that of the real Tropics has two maxima near the surface and the tropopause and takes relatively smaller value at the middle layer (Satoh and Hayashi, Fig. 12). Though streamlines will concentrate within the boundaries if one uses more realistic nongray schemes, the effects of the gray model—that is, the broad boundary layers of the Hadley cell and the lower tropopause—will not qualitatively alter subsequent arguments.

Figure 2 shows the meridional distributions of (a) the zonal wind, (b) the angular momentum (normalized by Ωa^2), and (c) the temperature in the standard case ($\Omega = \Omega_0$). Easterlies develop near the equator from the surface to the upper layers, and westerlies dominate in the poleward of the easterly region except for the bottom layers. In the poleward flow of the upper layers of the Hadley cell, the angular momentum is conserved and westerlies becomes stronger at higher latitudes. Maxima of the westerlies are located at the poleward boundaries of the Hadley cell. In the equatorward flow of the lower layers of the Hadley cell, the zonal wind is easterly in every latitude. In the stratosphere, the influence of the initial state remains as a weaker zonal wind in higher altitudes. The temperature is almost uniform in the latitudinal direction in the Hadley cell. In the poleward regions of the cells, atmospheric temperatures depend on the value of the surface

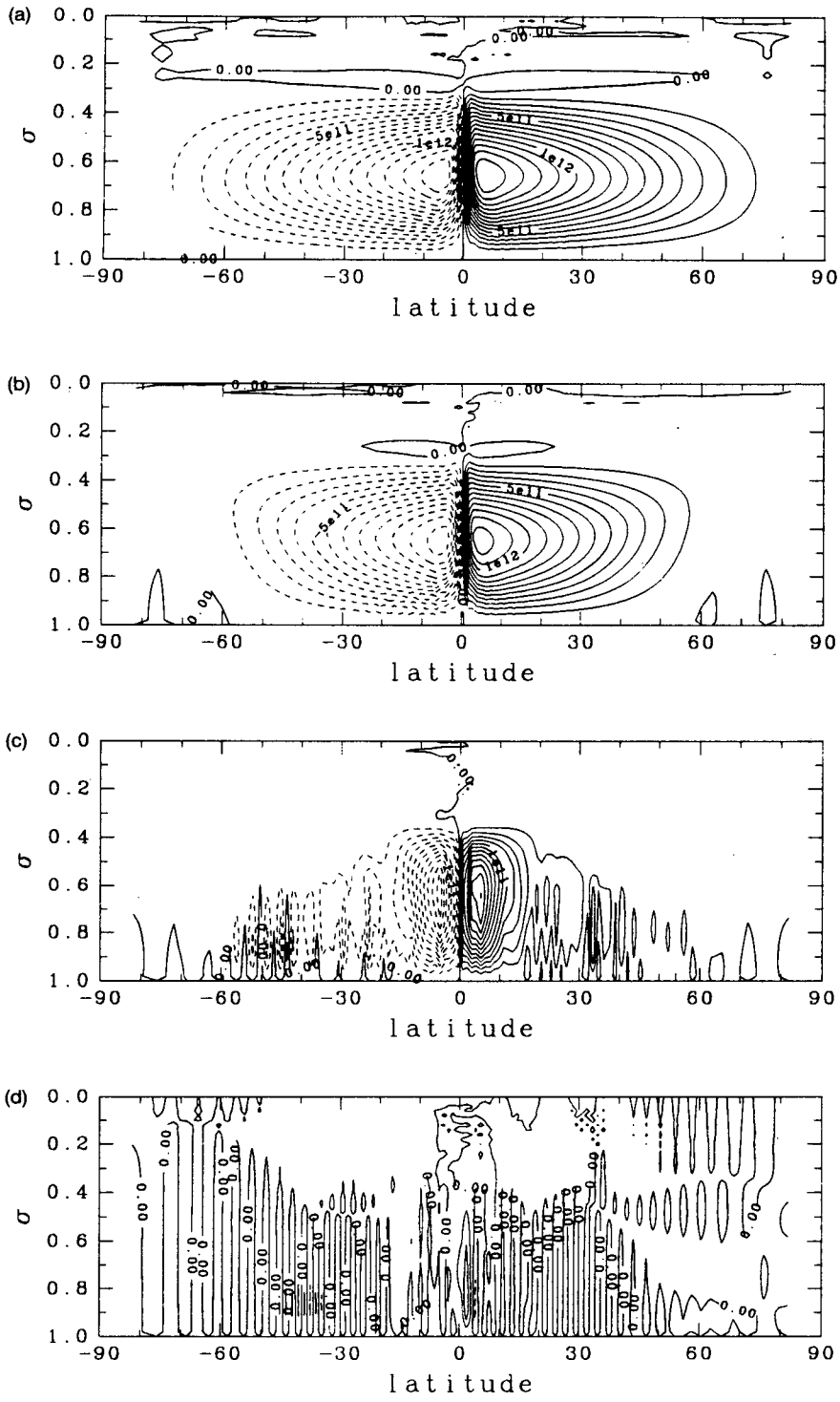

FIG. 1. Meridional distributions of mass streamfunction for Ω = (a) 0, (b) $0.1\Omega_0$, (c) Ω_0 (the standard case), and (d) $10\Omega_0$, where $\Omega_0 = 2\pi/(24 \times 60 \times 60)$ (rad s^{-1}) is the terrestrial rotation rate. Contour intervals are 1×10^{11} kg s^{-1} for (a) and (b), and 2×10^{10} kg s^{-1} for (c) and (d).

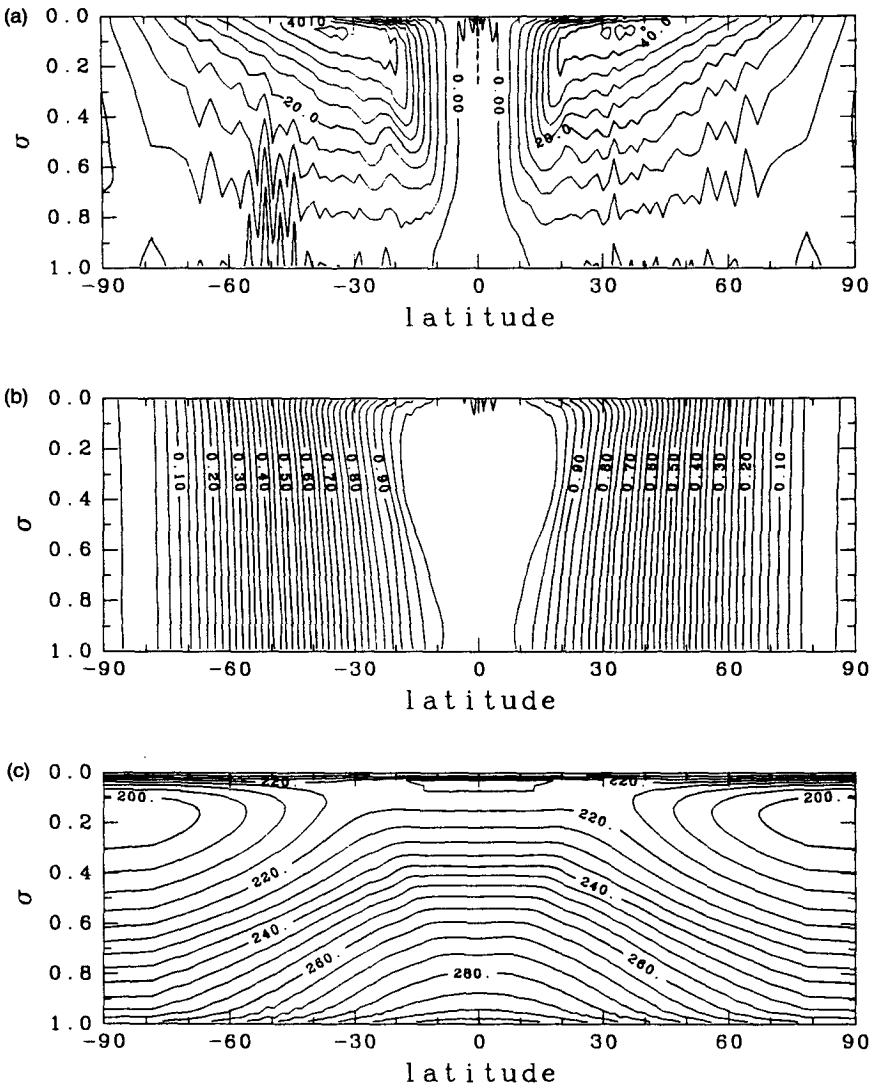

FIG. 2. Meridional distributions in the standard case of (a) zonal wind with a contour interval of 5 m s^{-1}, (b) absolute angular momentum normalized by the value at the equator Ωa^2 with a contour interval of 0.02, (c) temperature with a contour interval of 5 K.

temperature at the corresponding latitude, and temperature profiles are determined so as to satisfy the local radiative–convective equilibrium. Between the latitudinally uniform region of temperature and the local radiative–convective equilibrium region a sharp boundary exists that slopes from 10° in the lower layers to 20° at the tropopause.

The pressure distribution can be inferred from the zonal winds (Fig. 2a). Since the cyclostrophic balance is satisfied except for the equatorial region, the contour of $u = 0$ from about 6° in the upper layers to about 11° in the lower layers corresponds to a high pressure, that is, the "subtropical high." In the lowest level, however, there is no clear high pressure in the subtropics. Time-averaged surface pressure is highest at the poles.

The convection in middle and high latitudes has a systematic multicell structure. This is clearly shown by the time sequences of precipitation as Fig. 3. Though precipitation is seen in lower latitudes, moving convective cells also exist in higher latitudes. The scale of the cells is about 1000 km, and the cells move equatorward at a speed of about 1 m s^{-1}. The surface zonal winds are easterly on the equatorial side of the upward motion of each cell, while they are westerly on the poleward side. No latitudinal belt of a steady surface westerly exists. Pairs of high and low pressure centers move equatorward as the convective cells move. It must also be noted that influence of the initial condition vanishes after about 20 days of integration. This timescale is almost equal to the advective time of the Hadley cir-

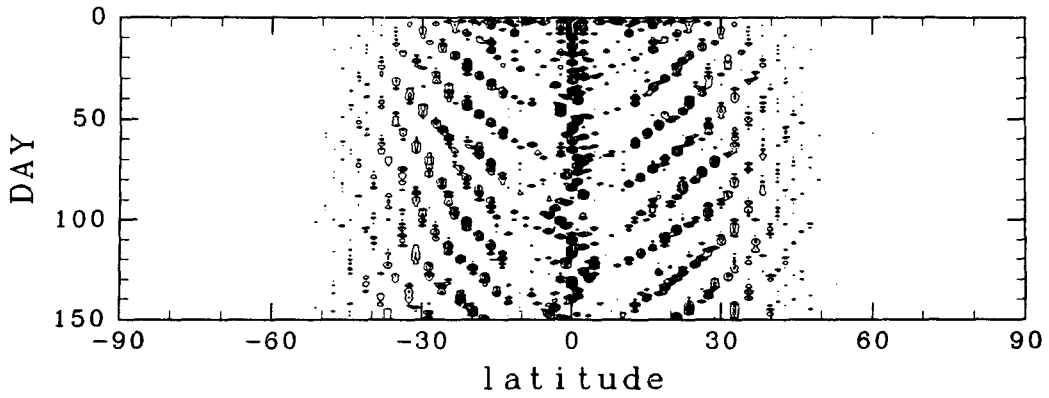

FIG. 3. Time sequences of precipitation in the standard case. The contour interval is 5×10^{-5} kg m^{-2} s^{-1}.

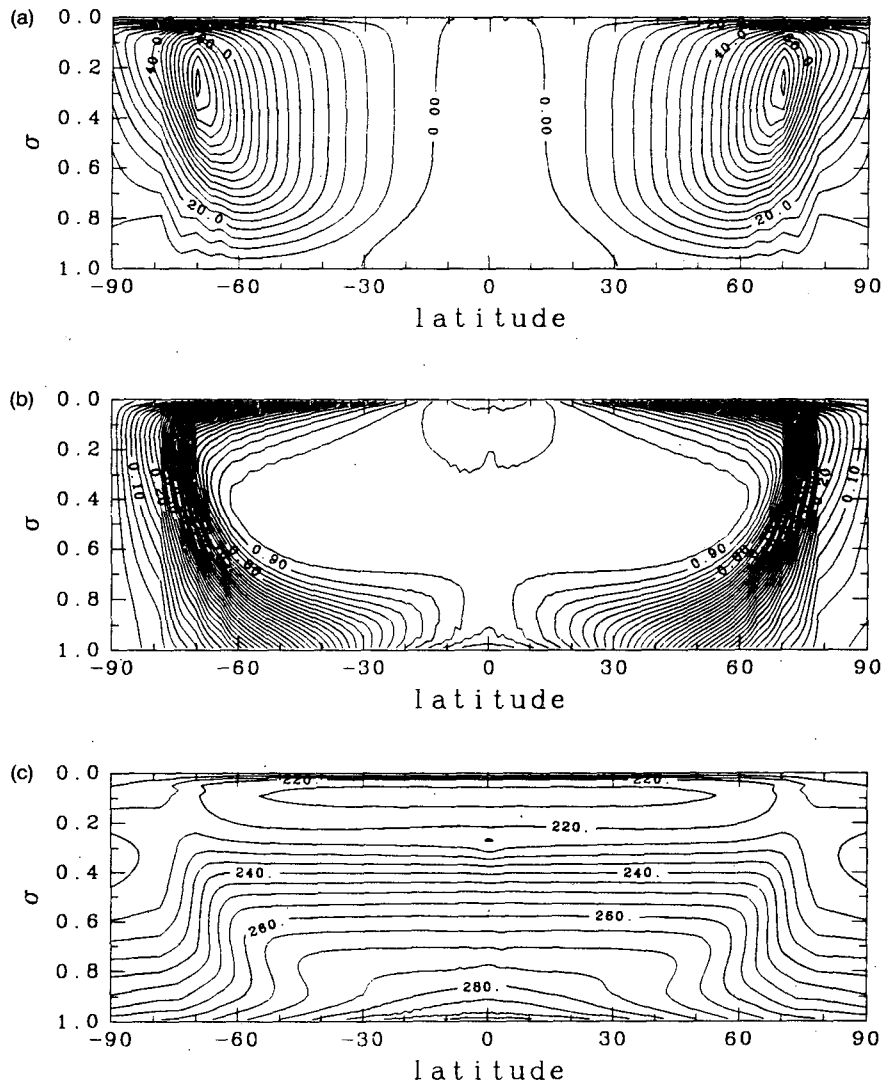

FIG. 4. As in Fig. 2 but for $\Omega = 0.1\Omega_0$.

culation, during which the width of the Hadley cell reaches the equilibrium state.

Figure 4 shows the meridional distributions of the zonal wind, the normalized angular momentum, and the temperature in the case of $\Omega = 0.1\Omega_0$. These distributions are similar to the standard case shown in Fig. 2, but this case displays a more "idealistic" structure of the Hadley circulation. In the poleward flow region of the upper layers extending from the equator to 60°, the angular momentum and the temperature are latitudinally uniform, while, in the equatorward flow region of the lower layers from the equator to 30°, the zonal winds are easterly. There is a sharp decrease in temperature at the poleward boundary of the Hadley cell.

Figure 5 shows a meridional distribution of the moist static energy $m \equiv C_pT + Lq + gz$ for $\Omega = 0.1\Omega_0$. Here m is almost uniform in the vertical column at the equator and in the upper layers of the Hadley circulation ($m = 3.1 \times 10^5$ J kg^{-1}). Since the column at the equator is nearly saturated in this case, the uniformity of m indicates that the vertical temperature profile is close to a moist adiabat. As shown by the contour $m = 3.0 \times 10^5$ J kg^{-1}, m is small in the middle troposphere in the midlatitudes. This is because the relative humidity is small in these latitudes. In summary, the vertical temperature profile in the upward motion region of the Hadley circulation is determined by the moist process to be a moist adiabat, and the profiles in the downward motion region have the same moist adiabat. The departure from uniformity of the moist static energy is ascribed to the distribution of the humidity, which has a distinct asymmetry between both regions.

b. *The fixed solar flux condition*

Experiments are also performed under the condition that the global energy budget is closed. The distribution of the solar flux is given as a seasonal average by

$$F_s(\varphi) = \left[1 - \Delta_F\left(\sin^2\varphi - \frac{1}{3}\right)\right]F_{s0}, \quad (27)$$

where $F_{s0} = 239.75$ W m^{-2} and $\Delta_F = 0.723$ is used (Lindzen 1990). The surface temperature is determined by the swamp condition.

When the swamp condition is used, circulation structures clearly depend on cumulus schemes through the interaction with the surface temperature. In the case of no cumulus parameterization, one-grid-scale disturbances develop in the lower atmosphere. In the case of cumulus adjustment, on the other hand, large-scale circulations are systematically built up regardless of the mixing ways of the angular momentum. These circulations do not depend on the grid size. For this reason, this subsection describes the experiments in which the convective adjustment scheme are used with the mixing of the angular momentum vertically during the adjustment process. More discussions on the differences among the cumulus schemes are given in the appendix.

Figure 6 displays the latitudinal distributions of the solar flux F_s and the outgoing planetary flux at the top of the atmosphere F_{pT} for $\Omega = 0$, 0.1, $1/\sqrt{10}$, 1, and $\sqrt{10}$ ($\times\Omega_0$). At the latitude where F_s agrees with F_{pT}, the latitudinal energy flux takes a maximum value. This latitude becomes higher as Ω decreases; it is about 20° when $\Omega = \Omega_0$, and is about 36° when $\Omega = 0$. Here F_{pT} is almost constant in the equatorial latitudes, which corresponds to the region of the Hadley circulation.

Figure 7 shows the distribution of the surface temperatures T_s for those values of Ω. The profiles of T_s are similar to those of F_{pT}. As Ω decreases, the surface temperature at the equator decreases, whereas it increases at the pole. However, detailed profiles near the equator are different for Ω. When $\Omega < \Omega_0$, the latitudinal gradient at the equator is discontinuous, while it is continuous when $\Omega = \Omega_0$. When $\Omega = \sqrt{10}\Omega_0$, the surface temperature has two maxima at 9° in both hemispheres and has a minimum at the equator.

The latitudes of the warmer surface temperature in Fig. 7 correspond to those where the upward motion exists. When the swamp condition is applied, the atmospheric circulations interact with the surface tem-

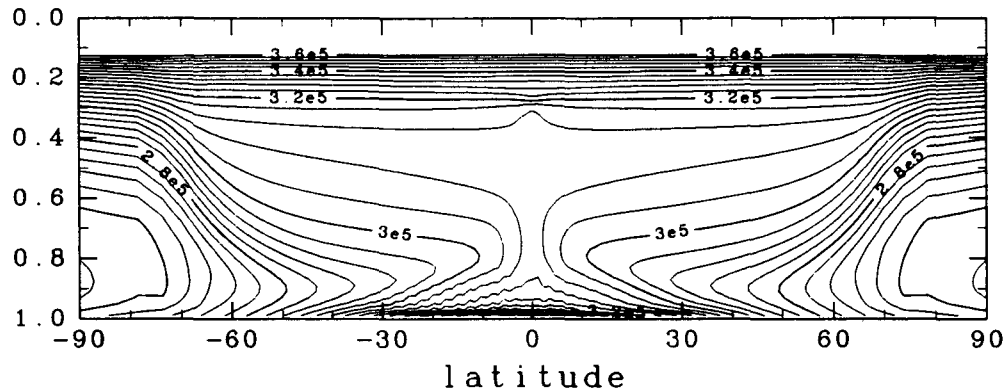

FIG. 5. Meridional distribution of moist static energy for $\Omega = 0.1\Omega_0$.

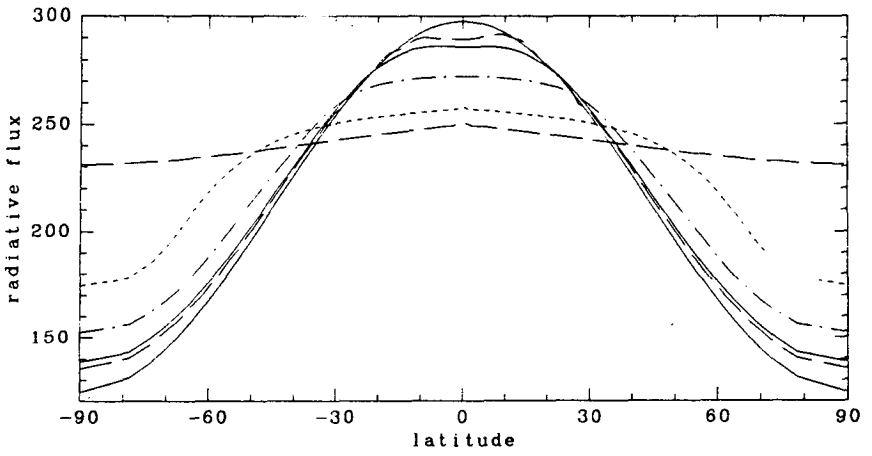

FIG. 6. Latitudinal distributions of the solar flux F_s and outgoing planetary fluxes at the top of the atmosphere F_{pT}. A curve that takes the largest value at the equator is F_s, and subsequent curves correspond to F_{pT} for $\Omega = \sqrt{10}, 1, 1/\sqrt{10}, 0.1$, and $0 (\times \Omega_0)$, respectively (units: W m^{-2}).

perature as following manners. At the lower levels of the upward motion region, water vapor is abundant, so the surface temperature becomes warmer owing to the constraint that the same amount of the energy as the surrounding latitudes must be supplied from the surface to the atmosphere. Conversely, the location of the upward motion tends to concentrate on the region of the warmer surface temperature.

The precipitations reflect the changes in the equatorial distribution of the surface temperature. Figure 8 displays the meridional distributions of the precipitations and the evaporations from the surface for $\Omega = \Omega_0$ and $(1/\sqrt{10})\Omega_0$. The evaporations have almost the same profile in two cases. The precipitation has a strong peak at the equator when $\Omega = (1/\sqrt{10})\Omega_0$, whereas it has two peaks in both hemispheres when $\Omega = \Omega_0$. For a faster rotation rate $\Omega = \sqrt{10}\Omega_0$, as shown in Fig. 7, the surface temperature also has two maxima at 9°, which correspond to peak latitudes of the precipitation.

4. Simple model

A simple model of the Hadley circulation in radiative–convective equilibrium is formulated here. First, the Hadley circulation is examined on the fixed temperature condition. In the second subsection, the fixed solar flux condition and the relation with HH80 and S77 are discussed.

a. Formulation

In the upper layers of the Hadley cell, the temperature is uniform in the latitudinal direction. The width of the Hadley cell φ_H is defined as the latitude to which the uniform temperature region extends at the tropopause $z = H$. The upward flows of the Hadley circulation are concentrated near the equator $\varphi \approx 0$, and the downward flows are almost uniform to φ_H. The vertical temperature profile in the upward motion region is moist adiabatic, and the profiles in the downward motion region are the same as in the upward motion region. These profiles of temperatures are understood in the simple framework presented by Satoh and Hayashi (1992).

The differences of the moist static energy and the specific humidity from the surface to the tropopause at the equator ($\varphi = 0$) are given by $\Delta m(0) = 0$, $\Delta q(0) \approx -q_B(0)$, where $q_B(0)$ is the surface specific humidity at the equator. If one writes $m = C_pT + Lq + gz \equiv C_p\theta + Lq$, then θ behaves like potential temperature. The corresponding difference of θ is approximately expressed by

$$\Delta\theta(0) = \frac{Lq_B(0)}{C_p}. \tag{28}$$

Equating this to a temperature drop due to the radiative cooling during a convective time τ_D, one finds

$$\tau_D = \frac{\Delta\theta(0)}{Q^{\text{rad}}/\rho C_p} = \frac{Lq_B(0)}{Q^{\text{rad}}/\rho}; \tag{29}$$

τ_D is defined as a time required for the flow to traverse the distance H. The downward mass flux per unit area in the downward motion region is expressed by $M^d = \rho H/\tau_D$. Hence one finds, using Eq. (29),

$$M^d = \frac{Q^{\text{rad}}H}{Lq_B(0)} \tag{30}$$

(Lindzen et al. 1982; Satoh and Hayashi 1992). Since M^d is almost constant from the equator to φ_H, the poleward mass flux V in the Hadley circulation is expressed by

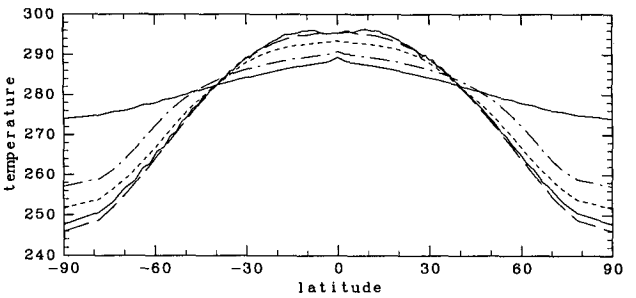

FIG. 7. Latitudinal distributions of surface temperatures for $\Omega = \sqrt{10}$, 1, $1/\sqrt{10}$, 0.1, and 0 ($\times\Omega_0$). The temperature at the equator decreases as the rotation rate becomes smaller. The unit is kelvin.

$$V(\mu) = \cos\varphi \int_{0\,v>0}^{H} \rho v dz = M^d a(\mu_H - \mu), \quad (31)$$

where $\mu \equiv \sin\varphi$, $\mu_H \equiv \sin\varphi_H$, and the conservation of mass is used. The integration of Eq. (31) is performed over the layers of positive meridional velocities. The maximum value of the streamfunction in Fig. 1 is expressed by $2\pi aV(0)$.

The poleward flow at the upper layer ($z = H$) conserves the angular momentum. Using the latitude φ_T ($\mu_T \equiv \sin\varphi_T$) where the zonal velocity vanishes in the level $z = H$, the angular momentum at $z = H$ is expressed by

$$l = \Omega a^2 \cos^2\varphi + u(\varphi, H) a \cos\varphi = \Omega a^2 \cos^2\varphi_T, \quad (32)$$

which reduces to

$$u(\mu, H) = \Omega a \frac{\mu^2 - \mu_T^2}{(1-\mu)^{1/2}}. \quad (33)$$

Integrating the equation of the angular momentum conservation (7) vertically, one obtains

$$\frac{1}{a\cos\varphi}\frac{\partial}{\partial\varphi}\left[\cos\varphi \int_0^H \rho v(\Omega a \cos^2\varphi + ua\cos\varphi)dz\right] = -a\cos\varphi\rho_s(C_DV)_m u(\varphi, 0), \quad (34)$$

where $u(\varphi, 0)$ is the zonal wind at the lowest level (u_1), and the small horizontal diffusion $\sigma'_{\lambda\varphi}$ has been neglected. Using $\int_0^H \rho v dz = 0$, and taking the contributions from the upper and lower levels of the zonal winds into account in the term including $ua\cos\varphi$, one can rewrite Eq. (34) as

$$\frac{\partial}{\partial\mu}\{V(\mu)[u_T(\mu) - u_B(\mu)](1-\mu^2)^{1/2}\} = -a(1-\mu^2)^{1/2}\rho_s(C_DV)_m u_B(\mu), \quad (35)$$

where quantities in the poleward flow near the tropopause are denoted by $(\ )_T$, those in the equatorward flow near the surface by $(\ )_B$, and $u(z = H) = u_T$ and $u(z = 0) = u_T$ are assumed here.[1] Substituting Eqs. (31) and (33) in this, one obtains, from the integration for $u_B(\mu)$,

$$u_B(\mu) = \Omega a \frac{\mu_H^2}{(1-\mu^2)^{1/2}}\left[\frac{3}{C+3}\left(1 - \frac{\mu}{\mu_H}\right)^2 - \frac{4}{C+2}\left(1 - \frac{\mu}{\mu_H}\right) + \frac{1}{C+1}\left(1 - \frac{\mu_T^2}{\mu_H^2}\right)\right], \quad (36)$$

[1] These are defined by $u_T \equiv \cos\varphi \int_{0,v>0}^{H} \rho v u dz/V$, $u_B \equiv \cos\varphi \times \int_{0,v<0}^{H} \rho v u dz/V$. Strictly, the assumptions $u(H) = u_T$, $u(0) = u_B$ are not acceptable, because the streamlines are not concentrated within the boundary layers as shown in Fig. 1. However, the errors are corrected by redefinition of the value of $(C_DV)_m$, so that the following arguments do not depend on these assumptions.

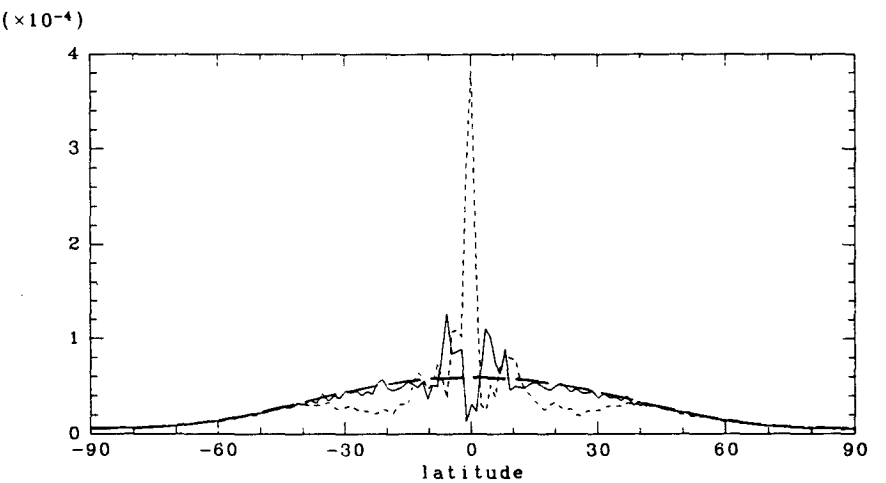

FIG. 8. Latitudinal distributions of precipitation and evaporation from the surface. Solid line: the precipitation for $\Omega = \Omega_0$; dotted line: the precipitation for $\Omega = (1/\sqrt{10})\Omega_0$; dashed lines: the evaporations, which are almost identical in both cases. The unit is kg m^{-2} s^{-1}.

where

$$C \equiv \frac{\rho_s (C_D V)_m}{M^d}. \tag{37}$$

Furthermore,

$$u_B(0) = u_T(0) \tag{38}$$

is assumed, since the angular momentum is conserved in the upward branch (at $\mu = 0$).

The latitude μ_T is given from Eqs. (33), (36), and (38). Equating (36) to zero, one also obtains the latitude μ_B, which is defined as the latitude where the zonal wind vanishes in the lowest level. These are

$$\mu_T = \left[\frac{2}{(C+2)(C+3)}\right]^{1/2} \mu_H \equiv r_1 \mu_H, \tag{39}$$

$$\mu_B = \frac{C + (C^2 + 6C + 12)^{1/2}}{3(C+2)} \mu_H. \tag{40}$$

One should pay attention to μ_T and μ_B since these correspond to the upper and lower positions of the subtropical high, respectively. If $C \gg 1$, then $\mu_T \approx 0$ and $\mu_B = (2/3)\mu_H$. If $C \ll 1$, then $\mu_T = \mu_B = (1/\sqrt{3})\mu_H$. Under the condition of surface slippery ($C = 0$), the angular momentum will have a uniform distribution in the Hadley cells, and the latitudes μ_T, μ_B will depend on the initial state. If the initial state is at rest, the average angular momentum of the rigid-body rotation over the cell is $\Omega a^2(1 - \mu_H^2/3)$, so that $\mu_T = \mu_B = (1/\sqrt{3})\mu_H$ is obtained. These values correspond to those in the limit $C \to 0$.

The latitude φ_H is determined by the cyclostrophic balance between the vertical shear of the zonal wind and the meridional gradient of the temperature. The region where the temperature is uniform extends from the equator to φ_H in the upper layers ($z = H$), while it extends to smaller latitudes in the lower layers. As a consequence, the vertically averaged temperature $\langle T \rangle$ has a meridional gradient. Since $u_T \gg u_B$ is satisfied in the latitudes from φ_T to φ_H, the bulk cyclostrophic balance is written as

$$\begin{aligned} -\frac{g}{T_0}\frac{1}{a}\frac{\partial \langle T \rangle}{\partial \varphi} &= \frac{1}{H}\left[2\Omega \sin\varphi u_T + \frac{\tan\varphi}{a} u_T^2\right] \\ &= -\frac{1}{H}\left[\frac{u_T}{a^2 \cos\varphi}\frac{\partial l_T}{\partial \varphi} - \frac{1}{a}\frac{\partial}{\partial \varphi}\frac{u_T^2}{2}\right] \\ &= \frac{1}{Ha}\frac{\partial}{\partial \varphi}\frac{u_T^2}{2}, \end{aligned} \tag{41}$$

where T_0 is the mean temperature in the troposphere, and Eq. (32) is used.

The vertical profiles of the temperature in the Hadley cell are the same as the moist adiabat at the equator $T(\varphi = 0, z)$, while the temperature profile in the poleward region of the Hadley cell follows a moist adiabat drawn from the surface temperature at the corresponding latitude. Thus, the vertically averaged temperatures are approximately expressed by

$$\langle T \rangle(\varphi_T) = T_s(0) - \Gamma_m \frac{H}{2}, \tag{42}$$

$$\langle T \rangle(\varphi_H) = T_s(\varphi_H) - \Gamma_m \frac{H}{2}, \tag{43}$$

where Γ_m is a typical value of the moist-adiabatic lapse rate. Integrating Eq. (41) over $\varphi_T < \varphi < \varphi_H$ and substituting Eqs. (26), (33), (42), and (43), one obtains

$$2R\mu_H^2 = \frac{(\mu_H^2 - \mu_T^2)^2}{1 - \mu_H^2}, \tag{44}$$

where

$$R \equiv \frac{gH\Delta_H}{\Omega^2 a^2}, \tag{45}$$

and $\Delta_H = (T_A - T_B)/T_0$. From Eqs. (39) and (44), one finds

$$\mu_H = \left[\frac{2R}{(1 - r_1^2)^2 + 2R}\right]^{1/2}. \tag{46}$$

In the limit of $R \ll 1$, $C \gg 1$ (i.e., $r_1 \ll 1$), this is approximated to

$$\mu_H = (2R)^{1/2}. \tag{47}$$

The latitudes φ_T, φ_B, and φ_H for the numerical experiments are compared with those from Eqs. (39), (40), and (46), as in Fig. 9a where the rotation rate Ω is changed, and as in Fig. 9b where the coefficient of surface viscosity ν_s is changed (ν_s = 0.1, 1, 5, 25, and 100 m^2 s^{-1}). The open circle, square, and triangle are φ_H, φ_B, and φ_T obtained from the simple model, respectively, and the solid ones are those from the numerical calculations. The dependencies of φ_H, φ_B, and φ_T to R for $C = 7.8$ are shown in (a) by the thick, dashed, and dotted lines, respectively, and the dependencies to C for $R = 0.068$ are also shown in (b). These values of R and C are those for the standard case. As the rotation rate decreases the width of the Hadley cell becomes broader. As the surface viscosity becomes smaller, the width becomes broader, though the dependency is weak. For the calculations of R and C, the values T_0 = 270 K, H = 10 km, ρ_s = 1 kg m^{-3}, and Δz = 200 m in Eq. (25) are used. Although M^d can be given by Eq. (30), M^d is estimated from the streamfunctions of the numerical results. The reason is that Q^{rad} in this equation does not have a definite value. Since Q^{rad} is a mean value of the radiative cooling over the Hadley circulation region, Q^{rad} becomes larger as the rotation rate is smaller (for broader Hadley cell), and then M^d becomes larger. For these experiments, M^d was within the range of 1–6 ($\times 10^{-3}$ kg m^{-2} s^{-1}).

b. Comparison with HH80 and other studies

The results of the previous subsection are very similar to the simple model of HH80, in which the Newtonian cooling and Boussinesq approximation were used. In this subsection, the relationship between HH80 and the present study will be discussed, especially in respect to the mechanism of the maintenance of the stratification, the width and the intensity of the Hadley cell, and the energy balance. The simple model on the fixed temperature condition is extended to the fixed solar flux condition.

The most distinct difference is the maintenance mechanism of the tropospheric stratification. In HH80, the Newtonian cooling keeps the distribution of the potential temperature close to the statically stable reference state θ_e. For the condition that the flow does not change the stratification of θ_e, HH80 required the inequality $\tau_D/\tau_R \gg 1$ [(21) (iv) of HH80], where τ_R is a relaxation time of the Newtonian cooling, and τ_D is a convective time. The stable θ_e is based on the assumption that small-scale moist convections maintain radiative–convective equilibrium in each latitude. It is not appropriate, however, to think of θ_e as incorporating the effect of moist convection, since the Hadley circulation suppresses the deep convections in the subtropics.

In this study, on the other hand, the internally calculated moist process controls the stratification: the temperature profile of the downward motion region of the Hadley cell is close to the moist-adiabatic profile in the upward motion region. Satoh and Hayashi (1992) have argued for the inequality $D/(S_h + LE) \ll 1$ in order for the temperature to be close to the moist adiabat; $S_h + LE$ is a sum of the sensible and the latent heat fluxes from the surface averaged over the Hadley cell. Here D should be regarded as an effective dissipation rate averaged over the whole domain of the Hadley circulation, although D in Satoh and Hayashi (1992) was estimated from the dissipation in deep cumulus. This inequity is generally satisfied in these experiments where $D = 1 \sim 5$ W m^{-2} and $S_h + LE \approx 100$ W m^{-2}.

The width of the Hadley cell, Eq. (47), is the same as Eq. (16) of HH80, $(5/3R)^{1/2}$, except for a constant factor. It should be noted, however, that Δ_H in the definition of R is a fractional latitudinal difference of T_s in this study, while it is that of θ_e in HH80. From the angular momentum budget, HH80 required the inequality $\tau_D/\tau_c \geq 1$ to satisfy $u(0) \ll u(H)$ [(21) (ii) of HH80], where $\tau_c \equiv H/(C_D V)_m$ is a timescale determined by the surface drag coefficient. Noting that $C = \tau_D/\tau_c$ from Eq. (37), one finds that the inequality $\tau_D/\tau_c \geq 1$ corresponds to $C \geq 1$. Under this condition, the easterlies at the equator are small enough for the angular momentum of the poleward flow of the Hadley cell to be approximated to Ωa^2. This implies that the angular momentum budget does not play an important role in determining the width of the Hadley cell in the case of $C \geq 1$.

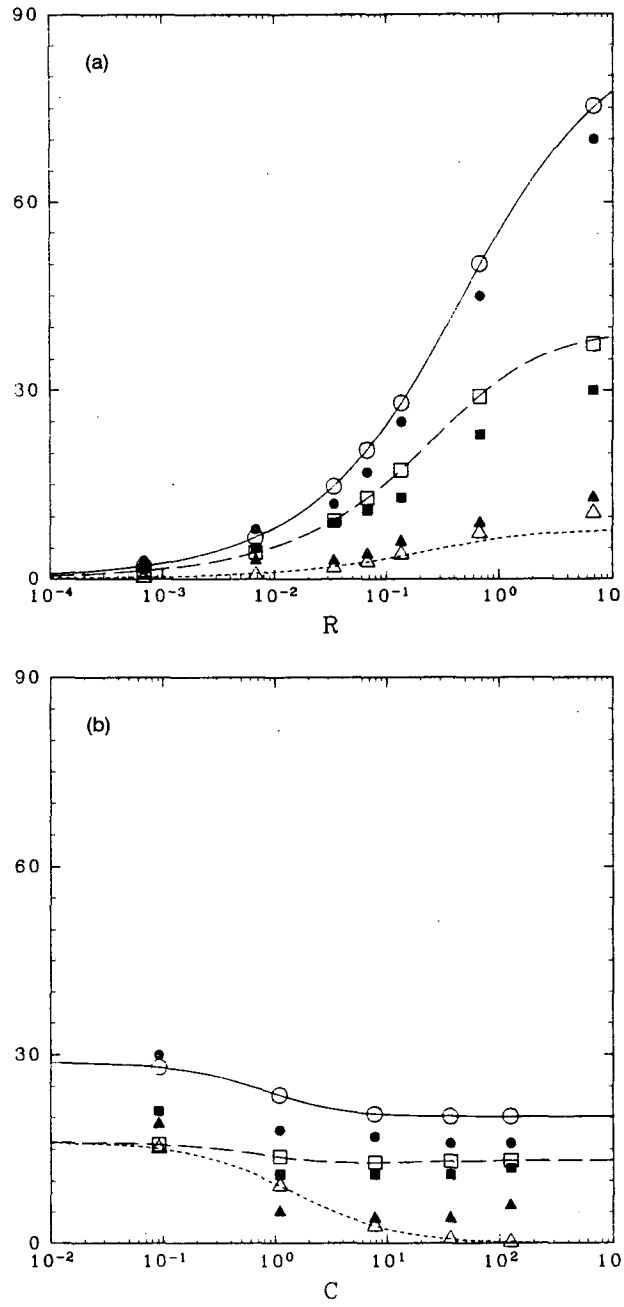

FIG. 9. Comparison of the latitudes φ_H, φ_T, and φ_B between numerical experiments and the simple model. Dependencies on (a) R and (b) C. Solid circles, squares, and triangles: numerical experiments; open circles, squares, and triangles: the simple model. Curves in (a) correspond to the case $C = 7.8$ calculated using the simple model, while in (b) $R = 0.068$; solid lines: φ_H, dashed lines: φ_T, dotted lines: φ_B.

From the requirement of the energy budget, HH80 determined the cell width and the value of the equatorial temperature. The method of HH80 is often referred to as an "equal areal" method (e.g., Lindzen 1990). In the previous subsection, on the other hand, the equatorial temperature profile is simply given by a moist adiabat from the specified surface temperature at the equator [Eq. (42)]. Therefore, the width of the Hadley cell can be determined without the requirement of the energy budget on the fixed temperature condition.

Under the fixed solar flux condition, however, the role of the energy budget becomes as important as in HH80. According to section 6 of HH80, the width of the Hadley circulation can be estimated on the assumption that the energy budget is closed in the region of the Hadley circulation. This assumption is generally inappropriate, since the solar flux exceeds the planetary flux in this region as shown by Fig. 6. Nevertheless, a major part of the energy transport in the middle and high latitudes is due to a weak meridional circulation caused by the imbalance from the cyclostrophy owing to the presence of the viscosity. Thus, one can approximately determine the width of the Hadley cell by considering the inviscid limit following HH80. HH80 also says that cases in which the moist processes exist can be considered in the framework of the Newtonian cooling (HH80, section 6; Hou and Lindzen 1992). In order to clarify this argument, the energy budget of the Hadley circulation, especially under the fixed solar flux condition, is examined here, on the basis of the consistent assumptions with HH80: $R \ll 1$ and $C \gg 1$.

The balance equation of the vertically averaged moist static energy m under the swamp conditions is given by

$$\frac{1}{\cos\varphi}\frac{\partial}{\partial\varphi}\int_0^\infty \cos\varphi \rho v m dz = -F_{pT} + F_s. \quad (48)$$

In general, the outgoing flux F_{pT} is a functional of the atmospheric temperatures and the surface temperature. It is approximately determined from the temperature at the level where the optical thickness τ^* is unity. If the potential temperature θ at this level is denoted by $\bar{\theta}$, one can write

$$F_s = A + B\theta_e, \quad (49)$$

$$F_{pT} = A + B\bar{\theta}, \quad (50)$$

where the coefficients A and B depend on the amounts of absorbing constituents, temperatures, etc. Equation (49) defines θ_e. By estimating the left-hand side of Eq. (48) from the contributions of the equatorward and the poleward flows of the Hadley circulation, one obtains

$$\frac{\partial}{\partial\mu}(V\Delta m) = -B(\bar{\theta} - \theta_e), \quad (51)$$

where $\Delta m \equiv \cos\varphi \int \rho v m dz/V \equiv m_T - m_B$ is the difference of m between the values near the tropopause and the surface. With the definitions $\Delta\theta \equiv \theta_T - \theta_B$ and $\Delta q \equiv q_T - q_B \approx -q_B$, Eq. (51) can be rewritten as

$$\frac{\partial}{\partial\mu}(V\Delta\theta) = -\frac{B}{C_p}(\bar{\theta} - \theta_e) + Q_L, \quad (52)$$

where

$$Q^L \equiv -\frac{L}{C_p}\frac{\partial}{\partial\mu}(V\Delta q) \approx \frac{L}{C_p}\frac{\partial}{\partial\mu}(Vq_B) \quad (53)$$

is the latent heat release. The simple model of HH80 is derived on the assumptions $Q^L = 0$. HH80 also say that the above equation can be extended to the moist case by defining

$$\tilde{\theta}_E \equiv \theta_e + \frac{C_P}{B}Q^L. \quad (54)$$

HH80 required the integration of Q^L over the domain to vanish (HH80, p. 531; see also Hou and Lindzen 1992). However, this assumption is inappropriate even under the swamp condition, because the net value of the integration of Q^L remains nonzero as latent heat release.

If the energy budget is closed within the Hadley circulation region $0 < \mu < \mu_H$, one obtains from Eq. (51)

$$\int_0^{\mu_H}(\bar{\theta} - \theta_e)d\mu = 0. \quad (55)$$

If $\bar{\theta}$ is regarded as the temperature at the middle of the troposphere $\langle T\rangle$ in Eq. (41) (neglecting a constant difference of $\Gamma_m H/2$), the same result as in HH80 is obtained, that is, the width of the Hadley cell is given by

$$\mu_H = \left(\frac{5}{3}R\right)^{1/2}, \quad (56)$$

where $\Delta_H = \Delta_F F_{s0}/BT_0$ in R [Eq. (45)]. In the standard case ($\Omega = \Omega_0$), one has $\varphi_H = 16.6°$ for $R = 0.049$, where $B = 5.4$ W m^{-2} K^{-1} is used.[2] The radiative damping time of HH80 is given by $\tau_R = C_p/B \times p_0/g$. Thus, $\tau_R \approx 1.9 \times 10^6$ sec, which is comparable to the convective time $\tau_D \approx H/w \approx 10^6$ sec. This implies that Eq. (21) (iv) of HH80 is inadequate.

The procedures of the calculations of the intensity of the Hadley cell are different between HH80 and the present study. The simple model of HH80 is derived on the assumptions $Q^L = 0$ and $\Delta\theta = T_0\Delta_v = \text{const}$ in Eq. (52). This means that Eq. (52) can be used for the calculation of the mass flux V. In the context of the

[2] The value of B is based on the results of one-dimensional calculations. This value can also be estimated from the relation between F_{pT} and T_s of Figs. 6 and 7 in the case of large Ω.

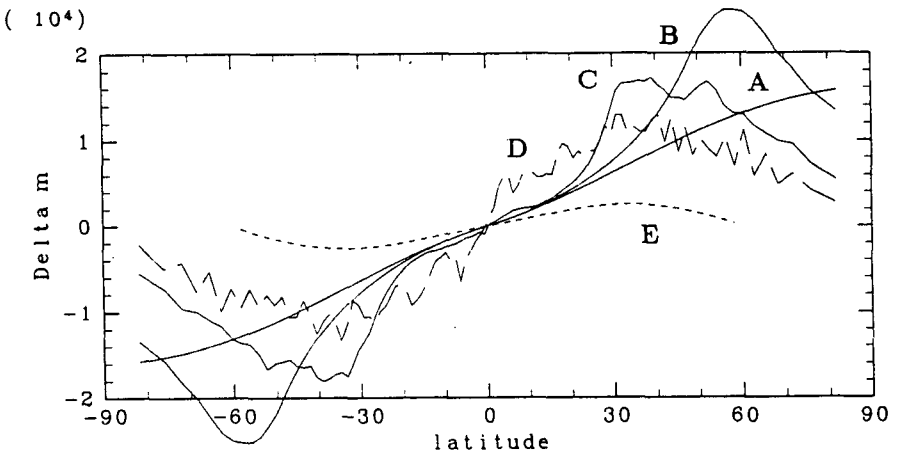

FIG. 10. Latitudinal distributions of differences of the upper and lower moist static energies Δm. Thick lines: $\Omega = 0$, 0.1, and $1/\sqrt{10}$ ($\times\Omega_0$) (denoted by A, B, and C, respectively); dashed line: $\Omega = \Omega_0$ (D); dotted line: $\Omega = (1/\sqrt{10})\Omega_0$ (E) by the simple model. The unit is J kg^{-1}.

present study, the mass flux is already give by Eq. (31), so that Eq. (51) can be used to estimate the latitudinal profile of Δm. Integration of Eq. (51) from 0 to μ gives

$$V\Delta m = B\int_0^{\mu}(\bar{\theta} - \theta_e). \tag{57}$$

From the estimation of the right-hand side by use of the results of HH80 [Eqs. (14a), (14b), (15), and (16), or Eq. (18) of HH80], one obtains

$$V\Delta m = \frac{5}{18}\left(\frac{5}{3}\right)^{1/2}\Delta_F F_{s0} a R^{3/2} \times\left\{\frac{\mu}{\mu_H} - 2\left(\frac{\mu}{\mu_H}\right)^3 + \left(\frac{\mu}{\mu_H}\right)^5\right\}. \tag{58}$$

By using Eqs. (31) and (56), one finds

$$\Delta m = \frac{1}{6}\left(\frac{5}{3}\right)^{1/2}\frac{\Delta_F F_{s0}}{M^d}\mu\left(1 - \frac{\mu}{\mu_H}\right)\left(1 + \frac{\mu}{\mu_H}\right)^2. \tag{59}$$

Held and Hoskins (1985) pointed out that Δm is an important quantity for considering the energy budget. Neelin and Held (1987) called it the gross moist stability, and discussed a method of calculating a divergence field of the flow by using observational Δm. However, it is reminded that this method should be diagnostically used and that it does not dynamically explain how the distribution of Δm is realized. In the present context, the surface temperature gradient determines the positions of the upward and downward motions, as a response to which the distributions of Δm or of water vapor are diagnostically determined.

Figure 10 shows latitudinal profiles of Δm for $\Omega = 0$, 0.1, $1/\sqrt{10}$, and 1 ($\times\Omega_0$). The sign of Δm is reversed in the latitudes $\varphi < 0$. The estimation by Eq. (59) is also added by a dotted line in the same figure for the case $\Omega = (1/\sqrt{10})\Omega_0$, where the values $\mu_H = \sin 60°$ and $M^d \approx 6 \times 10^{-3}$ kg m^{-2} s^{-1} are used based on the numerical result. For $\Omega/\Omega_0 < 1$, as is consistent with Eq. (59), gradients of Δm near the equator do not depend on Ω. For $\Omega/\Omega_0 = 1$, however, Eq. (59) is not a good estimation. In addition to this, Δm do not vanish at the poleward boundaries of the cells for all cases, since the energy budget is not closed within the Hadley circulation region. This implies that the above simple model underestimates Δm. For $\mu \ll 1$, Eq. (59) gives the gradient $d\Delta m/d\mu = (1/6)\sqrt{5/3}(\Delta_F F_{s0})/M^d \approx 6 \times 10^3$ J kg^{-1}, which is about half of those of the numerical experiments.

The above estimations are not a good approximation for the terrestrial condition. This is because, as shown in Fig. 6, the upward branches coexist in both hemispheres near the equator, and the Hadley circulation is not clearly defined. One might think that the terrestrial condition is a marginal case to which the simple model can be applied. Williams (1988a,b) compared the results of the axisymmetric calculations with those of three-dimensional calculations for GCM under the conditions of fixed solar flux and the swamp surface. The axisymmetric circulations of Williams (1988b) have complex cell structures, particularly in the case of the faster rotation rates. In the present research, similar to Williams (1988b), the structure of the Hadley cell is somewhat complicated (the double ITCZ) under the fixed solar flux condition. However, under the fixed surface temperature condition, a single cell structure with a strong upward motion exists at the equator, as shown in section 3a. The results of Williams may be caused by the stronger interaction between the surface temperature and the circulation in the axisymmetric model in comparison to the three-dimensional GCM.

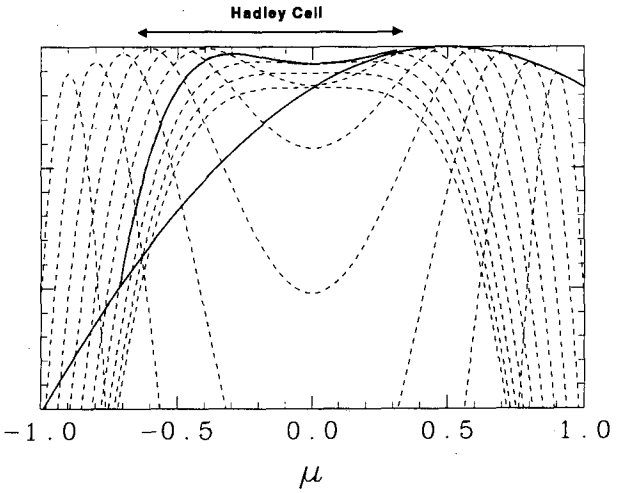

FIG. 11. Relationship between the surface temperature T_s (solid line) and temperatures in thermal wind balance with the upper-level angular momentum–conserving flow $\tilde{T}$ (dotted lines). The latitude of the maximum surface temperature is $\mu_0 = 0.5$ (30°). The upper flow is assumed to originate from the latitude μ_u where corresponding $\tilde{T}$ agrees with T_s. The Hadley circulation exists in the region shown by a thick envelope curve. The vertical coordinate is appropriately scaled.

Schneider (1977) examined the moist cases by fixing the surface temperature. The results of his numerical calculation, especially the meridional distribution of the temperature, is very similar to the present study. However, S77 used the Newtonian cooling and externally fixed the latitudinal distribution of the latent heat release. The assumption of the Newtonian cooling is essential to determine the width of the Hadley cell. The cell width is determined by the constraint of the energy balance {radiative cooling} = {latent heat release} [Eq. (20) of S77]. In the present study, the corresponding balance is used to obtain Eq. (30). One can derive the expression of the cell width of S77 by starting from Eq. (30), in which

$$\frac{Lq_B(0)}{H} = \frac{C_p\Delta\theta}{H} = \frac{C_pT_0N^2}{g}, \tag{60}$$

$$M^d = \rho\frac{H}{\tau_D}, \tag{61}$$

$$Q^{\text{rad}} = \frac{\rho C_pT_0}{\tau_R}\frac{\Omega^2a^2}{gH}\mu_H^4, \tag{62}$$

where N is the Brunt–Väisälä frequency of a moist adiabat. Equation (62) is derived by using the Newtonian cooling from the difference between the temperature in the cyclostrophic balance and the reference temperature. The nondimensionalized equation of this corresponds to the meridional average of Eq. (20) of S77. If these are inserted into Eq. (30), one obtains

$$\mu_H = \left(\frac{NH}{\Omega a}\right)^{1/2}\left(\frac{\tau_R}{\tau_D}\right)^{1/4}. \tag{63}$$

By following the appendix of S77, the essence of which is simply the assumption $\tau_R = \tau_D$, one can derive Eq. (21) of S77 except for a constant factor. The cell width is inversely proportional to $\Omega^{1/2}$ since the reference temperature θ_e is set to be constant regardless of the latitude. In HH80, in contrast, the width is inversely proportional to Ω since θ_e depends on μ^2.

5. Further results

a. Asymmetric condition centered off the equator

The Hadley circulation has been modeled under both fixed surface temperature condition and fixed solar flux condition. In the terrestrial case with the swamp surface, the Hadley cell does not have a clear structure because of the interaction between the surface temperature and the circulation. Thus, one will gain more information from the experiments on the prescribed surface temperature rather than from those under the prescribed solar flux. In this section, the cell width under the asymmetric condition centered off the equator will be particularly examined as a seasonal variation.

The simple model of section 4 is extended to the case where the surface temperature is asymmetric around the equator

$$T_s(\varphi) = T_A - (T_B - T_A)(\sin\varphi - \sin\varphi_0)^2, \tag{64}$$

where $\varphi_0 > 0$. Based on the numerical calculations shown later, further assumptions are introduced in addition to section 4; the upward motion is concentrated in a narrow region near φ_0, and the zonal wind of the upper layers vanishes at φ_0.

One obtains the poleward mass flux and the zonal winds at the lower and the upper levels by simply replacing μ_T by $\mu_0 \equiv \sin\varphi_0$ in Eqs. (31), (33), and (36). Integrating Eq. (41) from μ_0 to μ, and using Eqs. (33) and (45), one rewrites the cyclostrophic balance as

$$\frac{\tilde{T}(\mu)}{T_0} = \frac{T_s(\mu_0)}{T_0} - \frac{\Delta_H}{2R}\frac{(\mu^2 - \mu_0^2)^2}{1 - \mu^2}, \tag{65}$$

where $\tilde{T} = \langle T\rangle(\mu) + \Gamma_mH/2$. Setting $\tilde{T} = T_s$ at $\mu = \mu_H$, and using Eq. (64), one finds

$$2R(\mu_H - \mu_0)^2 = \frac{(\mu_H^2 - \mu_0^2)^2}{1 - \mu_H^2}, \tag{66}$$

which reduces to

$$\mu_{H\pm} = \pm\left[\frac{2R}{1 + 2R}\left(1 - \frac{\mu_0^2}{1 + 2R}\right)\right]^{1/2} - \frac{\mu_0}{1 + 2R}. \tag{67}$$

In general, two solutions exist; μ_{H+} is a solution for a summer cell, and μ_{H-} is for a winter cell. Note that the case of $\mu_0 = 0$ in (67) corresponds to the case of $C \gg 1$ in (46).

If $\mu_{H+} < \mu_0$, μ_{H+} is not an appropriate solution for a summer cell. In this case, furthermore, the atmospheric temperature $\tilde{T}$ in the equatorial side of μ_0 becomes lower than the surface temperature T_s. This situation contradicts the view that the meridional flows are driven by a latitudinal temperature gradient. If such a circulation is assumed, deep convections will occur in the wide range of the equatorial side because of the unstable stratification. Hence, the systematic meridional flows will no longer exist. It is thought, therefore, that the widths of the Hadley cells are given by (67) only when $\mu_0 < \mu_{H+}$ is satisfied. This condition is rewritten as

$$\mu_0 < \mu_{0S} \equiv \left(\frac{R}{2+R}\right)^{1/2}. \tag{68}$$

One obtains $\varphi_{0S} = \sin^{-1}\mu_{0S} = 9.8°$ under the terrestrial condition. Note that one can derive the inequality (68) from (8) of Plumb and Hou (1992), by replacing $\hat{T}_e$ by T_s [Eq. (64)] and evaluating at $\mu = \mu_0$.

In the case of $\mu_0 > \mu_{0S}$, no summer cell exists. As for the winter cell, the assumption that the position of the upward branch agrees with μ_0 will no longer be accepted. In this case, the range where the Hadley cell exists is determined by the following procedure. Replacing μ_0 by a latitude of the upward branch μ_u in (65), and giving various values for μ_u, one obtains the relations between $\tilde{T}$ and T_s as in Fig. 11. Here $\mu_0 = 0.5$ (30°) and $R = 0.1$ are used. For each μ_u, a meridional circulation exists only in the region where $\tilde{T} > T_s$ is satisfied adjacent to μ_u. The range where $\tilde{T} > T_s$ is satisfied is broadest for $\mu_u = 0.3$ (17.5°); it extends from μ_u to $\mu = -0.55$ (33.4°) in the winter hemisphere. This range is regarded as the region of the Hadley circulation for this profile of the surface temperature. The upward motion is located at about 17.5°. In the regions $\mu > 0.3$ and $\mu < -0.55$, there exists local radiative–convective equilibrium with small-scale vertical convections instead of a systematic meridional circulation.

In the next place, the distribution of the zonal winds near μ_0 will be examined. Substituting $\mu = \mu_T = \mu_0$ into Eq. (36), one obtains the surface winds near μ_0 as

$$u_B(\mu_0 \pm 0) = -\Omega a \frac{\mu_{H\pm}^2}{(1-\mu_0^2)^{1/2}} \frac{2C}{(C+1)(C+3)} \times \left[\frac{\mu_0}{\mu_{H\pm}} + \frac{1}{C+2}\right]. \tag{69}$$

In the polar side of the upward motion ($\mu_0 + 0$), the zonal wind is always easterly. In the equatorial side ($\mu_0 - 0$), it is westerly when $\mu_0/|\mu_{H-}| > 1/(C+2)$, while it is easterly when $\mu_0/|\mu_{H-}| < 1/(C+2)$. Since the angular momentum is conserved in the upward flow at μ_0, the upper-level zonal wind at μ_0 will be within the range of $u_B(\mu_0 + 0)$ and $u_B(\mu_0 - 0)$. Thus, in order for the upper-level zonal wind to vanish at μ_0, both inequalities $u_B(\mu_0 + 0) > 0$ and $u_B(\mu_0 - 0) < 0$ must be required. The condition $u_B(\mu_0 - 0) < 0$ is the same as $\mu_0/|\mu_{H-}| > 1/(C+2)$, which reduces to, from Eq. (67),

$$\mu_0 > \mu_{0C} \equiv \left[\frac{2R}{(C+1)^2 + 2R(C+2)^2}\right]^{1/2}. \tag{70}$$

One obtains $\varphi_{0C} = \sin^{-1}\mu_{0C} = 3.1°$ under the terrestrial condition.

It should be noted that, by setting $\mu = 0$, $\mu_T = \mu_0$ and $\mu_H = \mu_{H-}$ in Eq. (36), one finds

$$u_B(0) = -\Omega a \frac{\mu_{H-}^2}{C+1}\left[\frac{2C}{(C+2)(C+3)} + \frac{\mu_0^2}{\mu_{H-}^2}\right] < 0. \tag{71}$$

That is, the surface wind at the equator is always easterly. This contrasts with the simple model of Lindzen and Hou (1988), where the surface wind at the equator is westerly; therefore it contradicts Hide's theorem (Hide 1969; S77; HH80). Lindzen and Hou (1988) have neglected the term including $u(\varphi, 0)$ in the left-hand side of Eq. (34). Their approximation does not yield a good estimation of the surface winds.

Figure 12 compares the dependencies of the Hadley circulation widths $\varphi_{H\pm}$ of the numerical calculations with those of the simple model [Eq. (67)]. It also shows the latitudes of the intense upward motions $\dot{\sigma} < -1 \times 10^{-6}\ \mathrm{s}^{-1}$ and φ_T. [Here, φ_T is calculated from Eq. (32) using a value of the angular momentum of the upper poleward flow, so that it represents a latitude from which the upper flow is supplied.] The results of the numerical calculations have the following properties. The upward branch of the Hadley cell is located near φ_0 when $\varphi_0 < 10°$, the summer cell becomes ambiguous when $\varphi_0 > 6°$, and the winter cell remains in almost the same size extending from +20° to −30° when $\varphi_0 > 10°$. The latitude φ_T is located in the middle of the intense upward motion region when $\varphi_0 > 3°$, while φ_T is greater than φ_0 when $\varphi_0 < 3°$, that is, the zonal wind at the upward branch is easterly. From a comparison with the simple model, $\varphi_{H\pm}$ of the numerical results agree well with Eq. (67) when $3° < \varphi_0 < 10°$. The values $\varphi_{0S} = 10°$ and $\varphi_{0C} = 3°$ also agree with the estimations from Eqs. (68) and (70).

b. Circulations in the middle and high latitudes

The scale of convective cells in the middle and high latitudes as shown in Fig. 3 can be estimated by a similar procedure to the Hadley cell. Strictly speaking, the

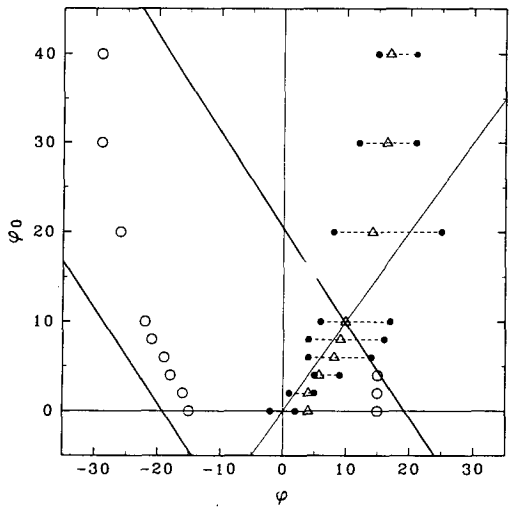

FIG. 12. Comparison of the characteristic latitudes of the Hadley circulation between numerical experiments and the simple model. The vertical coordinate and a thin solid line: the latitude of the maximum surface temperature φ_0; thick solid lines: the width of the Hadley cell φ_H from the simple model; white circles: φ_H from numerical experiments; dotted lines between black circles: latitudes of the intense upward motions $\dot{\sigma} < -1 \times 10^{-6}\ s^{-1}$; white triangles: φ_l calculated from the upper-level angular momentum l by $l = \Omega a^2 \cos^2\varphi_l$.

model of the previous sections is not applicable to the transient flows of the equatorward-moving cells because the model is based on a Lagrangian properties of the angular momentum. However, Fig. 3 shows that all precipitating regions are stationary in about ten days, and new regions successively emerge in the equatorward sides only after the old ones weaken. The scale of the cells is determined in this stationary phase. Thus, the argument on the steady circulation can be used to the first approximation.

For each cell, the upper-level flow conserves angular momentum. From the thermal wind balance, one obtains

$$f\frac{\partial u}{\partial z} = \frac{g}{T_0}\frac{\partial \langle T\rangle}{\partial y}, \tag{72}$$

where f is the Coriolis factor, and y is the latitudinal length. Using $u = fy$, $y \approx L$, $z \approx H$, and $d\langle T\rangle/dy \approx dT_s/dy$, one obtains a meridional scale

$$L = \frac{gH}{f^2 T_0}\frac{dT_s}{dy} \equiv \frac{H\Lambda}{f}, \tag{73}$$

where Λ is a mean vertical shear of the zonal winds. The scales of the Hadley circulation and of the convective cells are clearly shown in terms of the relations between T_s and $\tilde{T}$ as in Fig. 13. A curve $\tilde{T}$ that starts from $T_s(0)$ crosses again with T_s at $\mu = (2R)^{1/2}$, which corresponds to the width of the Hadley cell [Eq. (47)]. The regions where $\tilde{T} > T_s$ is satisfied in mid- and high latitudes correspond to the scales of the convective cells.

The propagation speed of the convective cells is about L/τ_D; they move one horizontal scale length while the air circulates one cycle of convection. The convective cells transport energy poleward and upward, and they transport angular momentum poleward and downward. Emanuel (1982) has shown that there is a symmetric mode propagating toward a warmer region due to wave–CISK in a sheared flow. The convective cells appeared in the present study have similar properties to Emanuel, but they also exist in dry experiments (see appendix).

6. Summary and further comments

Using an idealistic axisymmetric model with the moist process, the Hadley circulation in radiative–convective equilibrium is investigated. The properties of the Hadley circulation are most clearly understood under the condition of the fixed surface temperature. In the region of the Hadley circulation, the vertical profiles of the temperature are close to the moist adiabat of the region of the upward motion, and the temperature becomes uniform in the latitudinal direction. A sharp meridional gradient of temperature is concentrated in the poleward boundary of the Hadley cell. The upper-level poleward flow conserves angular momentum, and the vertical shear of the zonal wind is in cyclostrophic balance with the meridional gradient of the vertically averaged temperature. The width of the Hadley cell can easily be predicted from the relationship between the

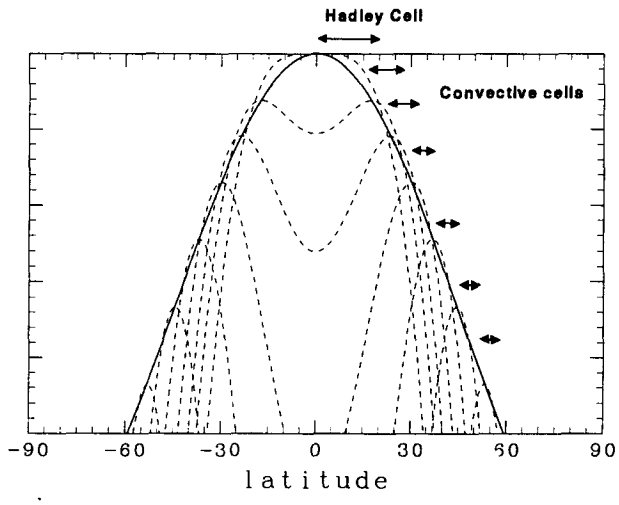

FIG. 13. As in Fig. 11 for $\mu_0 = 0$. The figure shows the scales of the Hadley cells and the convective cells in middle and high latitudes. The Hadley cell exists in the region where the dotted line that starts from $T_s(0)$ (the solid line at the equator) is located above the solid line. The region where each dotted line is located above the solid line in middle and high latitudes corresponds to the scale of a convective cell.

profiles of the surface temperature and the vertically averaged temperature (see Figs. 11, 13).

In the case where the solar flux is fixed, one can approximately determine the cell width on the assumption that the energy budget is closed in the cell. This result supports the simple model of Held and Hou (1980). However, the cell does not have a clear structure in the terrestrial case because of the interaction between the circulation and the surface temperature. In particular, in the case where the rotation rate is faster than or equal to the terrestrial value, two peaks of the upward branch of the Hadley cell appear in both hemispheres near the equator.

One should note that the model for the fixed solar flux condition is not a good approximation for the real atmosphere. Observationally, the solar flux exceeds the planetary flux in the region of the Hadley circulation, which extends to 30° (e.g., Fig. 1 of Vonder Haar and Suomi 1971). The latitudinal energy transport of the atmosphere–ocean system has its maximum at the polar boundary of the Hadley cell. The energy transports in the middle and high latitudes are about 5×10^{15} W, in which the eddy component occupies a larger part (Oort and Peixóto 1983). The eddy transport is smaller compared with the total heating by the release of latent heat in the Hadley cell 2×10^{16} W, but it amounts to 40 W m^{-2} for a unit area (after Lorenz 1967). Thus, the axisymmetric model gives an underestimation of the Hadley circulation width.

In the middle and high latitudes, a systematic cellar structure moving equatorward exists. Neither an indirect cell, nor a steady surface westerly belt, nor a subtropical high pressure at the ground level exists. These moving cells have an important role in the angular momentum balance in this symmetric system. The angular momenta are supplied from the ground in the region of the Hadley circulation where the surface winds are easterly, and are transported upward and poleward by the Hadley circulation. These are balanced with the downward transport by the moving cells, which is in contrast with the classical view of the symmetric circulation, in which the transport by the Hadley cell was thought to be balanced with an indirect cell in the middle and high latitude (the Ferrel cell). Such moving cells are idealistic in the symmetric system. The Richardson number Ri in middle and high latitudes is greater than one because of the moist-adiabatic stratification and the thermal wind balance with the prescribed meridional temperature gradient, so this symmetric state is in general baroclinically unstable (Stone

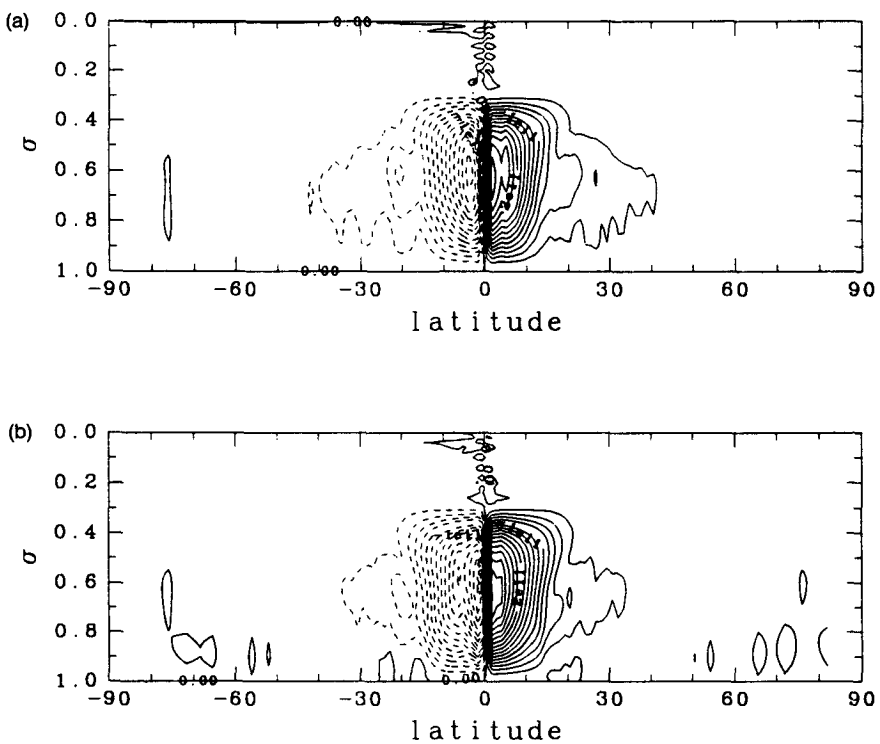

FIG. A1. Dependences of mass streamfunctions on the convective schemes under the fixed surface temperature condition for $\Omega = \Omega_0$ and moist experiments. (a) The adjustment scheme with angular momentum mixing; (b) the adjustment scheme without angular momentum mixing. Contour intervals are 2×10^{10} kg s^{-1}

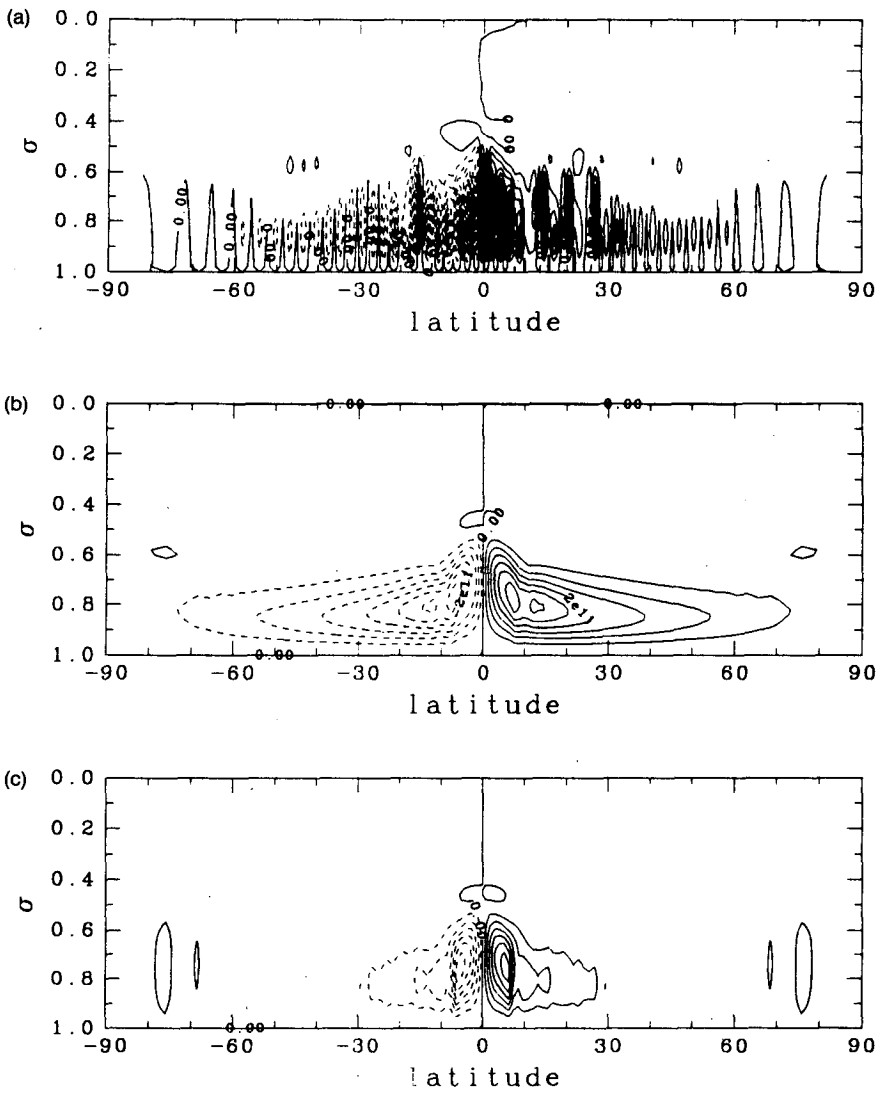

FIG. A2. As in Fig. A1 for dry experiments. (a) The scheme with no parameterization of convection; (b) the adjustment scheme with angular momentum mixing; (c) the adjustment scheme without angular momentum mixing. Contour intervals are 1×10^{11} kg s^{-1} for (a), and 5×10^{11} kg s^{-1} for (b) and (c).

1966). It is, however, worthwhile to examine the dynamics of the symmetric cells, because these cells may appear in the situations where Ri is less than one (for instance, the stratification is nearly neutral).

The symmetric results of the present study should be compared with the asymmetric ones in the same boundary conditions with the same physical processes. In particular, interactions between the Hadley circulation and the baroclinic waves should be examined, that is, how much baroclinic instability affects the width and the strength of the Hadley circulation and the zonal wind distributions. Actually, only through these comparisons is the meaning of the studies of the Hadley circulation in the symmetric condition verified.

Acknowledgments. The author thanks Prof. T. Matsuno for his continuing encouragement and many useful comments. The author also thanks Prof. A. Arakawa, Prof. Y. Matsuda, Dr. Y.-Y. Hayashi, and Dr. A. Numaguti for several useful discussions. The author also appreciates the comments by Prof. I. Held and an anonymous reviewer for the improvement of this paper. Numerical calculations were performed by HITAC S-820 and M-680H at the Computer Center of the University of Tokyo, and NEC SX-3 at the National Institute for Environmental Studies. Figures were produced by GFD-DENNOU libraries and GTOOL3 by Dr. Numaguti. This work was supported by the Japan Society for the Promotion of Science.

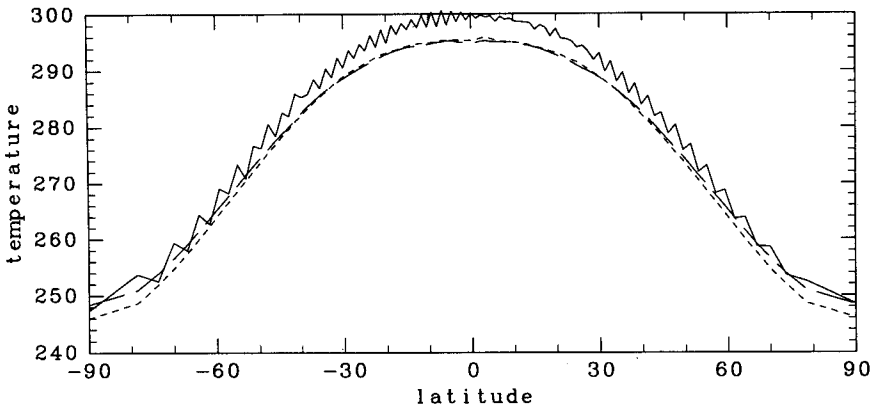

FIG. A3. Dependencies of surface temperatures on the convective schemes under the fixed solar flux condition for $\Omega = \Omega_0$ and moist experiments. Solid line: the scheme with no parameterization of convection; dashed line: the adjustment scheme with angular momentum mixing; and dotted line: the adjustment scheme without angular momentum mixing. The unit is kelvin.

APPENDIX

Dependencies on the Convective Schemes

The dependencies of the mass streamfunctions on the convective schemes are shown in Fig. A1. These are the results of the moist experiments for $\Omega = \Omega_0$ under the fixed surface temperature condition. The convective schemes compared are 1) the scheme with no parameterization of convection (except for the large-scale condensation; see Fig. 1c); 2) the adjustment scheme with angular momentum mixing; and 3) the adjustment scheme without angular momentum mixing. The figures show that the circulations do not depend on the convective schemes; clear Hadley cells exist in the low latitudes, and a multicell structure moving equatorward exists in middle and high latitudes.

The streamfunctions for the dry experiments are shown in Fig. A2. In case 1, one-grid-scale convective cells dominate in every latitude, while in cases 2 and 3, they are smoothed out by the adjustment process. The meridional circulation extends to the pole in case 2, whereas it is confined to lower latitudes in case 3. The averaged intensity over several latitudinal grid points in case 1 has almost the same profile as in case 2. In every case, the intensities of the meridional circulations are strong from the equator to about 10°. In case 3, there are no time-averaged meridional cells in middle and high latitudes. This is because the convective cells are moving equatorward in these latitudes, similar to the moist experiments. It is suggested that the vertical transport of the angular momentum is a key role for the propagation of the cells, since the adjustment scheme of case 3 does not mix angular momentum vertically.

In moist experiments, the effect of the convective schemes is not significant. Moist convection is organized in such a way that it has a resolvable horizontal scale in the model. Thus, the energy and the angular momentum are transported consistently by the "large-scale flow," and the stratification is stabilized even if no cumulus parameterization is used. The adjustment process does not alter the large-scale flows, since the adjustment process occurs in the lower layers. Tiedke (1988) has also reported that the results of three-dimensional GCMs for the case where no cumulus parameterization is employed are similar to those for the case where the convective adjustment scheme is used.

In dry experiments, on the other hand, the effect of the adjustment schemes is prominent. If no adjustment schemes are employed, one-grid-scale convective cells dominate. Convection in a dry atmosphere tends to have an aspect ration of 1:1 by analogy with the Benard convection, so that they have the smallest scale in the model. Convective adjustment is substituted for the roles of such a kind of small-scale convection.

The dependencies on the convective schemes are further influenced by the surface conditions. In moist experiments with no adjustment schemes under the fixed solar flux condition, there exist remarkable one-grid-scale convective cells similar to those in the dry experiments. In this case, the surface temperature is affected by the atmospheric circulation, so that the intensity of smaller-scale cells tends to be strengthened. The amplitude of one-grid-scale disturbance of the surface temperature amounts to about 5 K (Fig. A3). However, the latitudinal energy transports do not depend on the convective schemes.

REFERENCES

Arakawa, A., and M. J. Suarez, 1983: Vertical differencing of the primitive equations in sigma coordinates. *Mon. Wea. Rev.*, **111**, 34–45.

Emanuel, K. A., 1982: Inertial instability and mesoscale convective systems. Part II: Symmetric CISK in a baroclinic flow. *J. Atmos. Sci.*, **39,** 1080–1097.

Goody, R. M., and Y. L. Yung, 1989: *Atmospheric Radiation. Theoretical Basis.* Oxford University Press, 519 pp.

Held, I. M., and A. Y. Hou, 1980: Nonlinear axially symmetric circulations in a nearly inviscid atmosphere. *J. Atmos. Sci.*, **37,** 515–533.

——, and B. J. Hoskins, 1985: Large-scale eddies and the general circulation of the troposphere. *Advances in Geophysics,* Vol. 20, Academic Press, 3–31.

Hide, R., 1969: Dynamics of the atmosphere of the major planets with an appendix on the viscous boundary layer at the rigid bounding surface of an electrically conducting rotating fluid in the presence of a magnetic field. *J. Atmos. Sci.*, **26,** 841–853.

Hou, A. Y., 1984: Axisymmetric circulations forced by heat and momentum sources: A simple model applicable to the Venus atmosphere. *J. Atmos. Sci.*, **41,** 3437–3455.

——, and R. S. Lindzen, 1992: The influence of concentrated heating on the Hadley circulation. *J. Atmos. Sci.*, **49,** 1233–1241.

Hunt, B. G., 1973: Zonally symmetric global general circulation models with and without the hydrologic cycle. *Tellus,* **25,** 337–354.

Landau, L. D., and E. M. Lifshitz, 1987: *Fluid Mechanics,* 2nd ed. Pergamon, 540 pp.

Lindzen, R. S., 1990: *Dynamics in Atmospheric Physics.* Cambridge University Press, 310 pp.

——, and A. Y. Hou, 1988: Hadley circulations for zonally averaged heating centered off the equator. *J. Atmos. Sci.*, **45,** 2416–2427.

——, ——, and B. F. Farrell, 1982: The role of convective model in calculating the climate impact of doubling CO_2. *J. Atmos. Sci.*, **39,** 1189–1205.

Lorenz, E., 1967: The nature and theory of the general circulation of the atmosphere. World Meteorological Organization, 161 pp.

Manabe, S., and F. Möller, 1961: On the radiative equilibrium and heat balance of the atmosphere. *Mon. Wea. Rev.*, **89,** 503–532.

——, and R. F. Strickler, 1964: Thermal equilibrium of the atmosphere with a convective adjustment. *J. Atmos. Sci.*, **21,** 361–385.

——, J. Smagorinsky, and R. F. Strickler, 1965: Simulated climatology of a general circulation model with a hydrologic cycle. *Mon. Wea. Rev.*, **93,** 769–793.

Neelin, J. D., and I. M. Held, 1987: Modeling tropical convergence based on the moist static energy budget. *Mon. Wea. Rev.*, **115,** 3–12.

Oort, A. H., and J. P. Peixóto, 1983: Global angular momentum and energy balance requirements from observations. *Advances in Geophysics,* Vol. 25, Academic Press, 355–490.

Plumb, A., and A. Y. Hou, 1992: The response of a zonally symmetric atmosphere to subtropical thermal forcing: Threshold behavior. *J. Atmos. Sci.*, **49,** 1790–1799.

Ramanathan, V., and J. A. Coakley, Jr., 1978: Climate modeling through radiative–convective models. *Rev. Geophys. Space Phys.*, **16,** 465–489.

Riehl, H., and J. S. Malkus, 1958: On the heat balance of the equatorial trough zone. *Geophisica,* **6**(3), 503–538.

Sarachik, E. S., 1978: Tropical sea surface temperature: An interactive one-dimensional atmosphere–ocean model. *Dyn. Atmos. Oceans,* **2,** 455–469.

Satoh, M., and Y.-Y. Hayashi, 1992: Simple cumulus models in one-dimensional radiative convective equilibrium problems. *J. Atmos. Sci.*, **49,** 1202–1220.

Schneider, E. K., 1977: Axially symmetric steady-state models of the basic state for instability and climate studies. II. Nonlinear calculations. *J. Atmos. Sci.*, **34,** 280–296.

——, 1983: Martian great dust storms: Interpretive axially symmetric models. *Icarus,* **55,** 302–331.

——, and R. S. Lindzen, 1976: A discussion of the parameterization of momentum exchange by cumulus convection. *J. Geophys. Res.*, **81,** 3158–3160.

——, and ——, 1977: Axially symmetric steady-state models of the basic state for instability and climate studies. I. Linearized calculations. *J. Atmos. Sci.*, **34,** 263–279.

Stone, P. H., 1966: On non-geostrophic baroclinic stability. *J. Atmos. Sci.*, **23,** 390–400.

Tiedtke, M. T., 1984: The effect of penetrative cumulus convection on the large-scale flow in a general circulation model. *Beitr. Phys. Atmosph.*, **57,** 216–239.

Vonder Haar, T. H., and V. E. Suomi, 1971: Measurements of the earth's budget from satellites during a five-year period. Part I: Extended time and space means. *J. Atmos. Sci.*, **28,** 305–314.

Williams, G. P., 1988a: The dynamics range of global circulations I. *Climate Dyn.*, **2,** 205–260.

——, 1988b: The dynamics range of global circulations II. *Climate Dyn.*, **3,** 45–84.